Development of Low Expansion Glaze Coatings on As Fired Si_3N_4 to Enhance Room Temperature Flexural Strength

by

Nandita N. Majumdar

Thesis submitted to the Faculty of the
Virginia Polytechnic Institute and State University
in partial fulfillment of the requirements for the degree of
Master of Science
in
Materials Science and Engineering

Dr. D. A. Hirschfeld, Chairman
Dr. J. J. Brown, Jr.
Dr. R. S. Gordon

19 June 1998
Blacksburg, Virginia

Keywords: silicon nitride, glaze coating, room temperature flexural strength

Development of Low Expansion Glaze Coatings on As Fired Si_3N_4 to Enhance Room Temperature Flexural Strength

by

Nandita N. Majumdar

Deidre A. Hirschfeld, Chairman

Materials Science and Engineering

(ABSTRACT)

Silicon nitride (Si_3N_4) has the potential for use in various high-performance applications. However, surface defects such as voids/pits are commonly present on as processed Si_3N_4. When subjected to external forces, fracture originates at such flaws. To reduce or eliminate surface flaws, machining operations are required which constitute a major proportion of production costs. In order to offer an inexpensive alternative to machining and also to enhance the room temperature flexural strength of as fired Si_3N_4, low expansion glaze coatings of lithium aluminosilicate (LAS) and magnesium aluminosilicate (MAS) compositions were developed. Homogeneous and crack-free glaze coatings were successfully formed on as processed Si_3N_4. This ensured formation of compressive surface stresses on the as fired Si_3N_4 which, in turn, led to the reduction of the effects of surface flaws. When compared to the uncoated as fired Si_3N_4, both the glaze coatings helped achieve greater flexural strength. Analyses of the two glazes indicated better strength for the MAS coating compared to the LAS. Wear tests revealed that the MAS glaze exhibited higher wear resistance than the LAS glaze. These differences were attributed to the ability of the magnesium aluminosilicate glaze to achieve greater surface smoothness and better adherence to the substrate than the lithium aluminosilicate.

Acknowledgements

I wish to express my gratitude to my advisor Dr. Deidre A. Hirschfeld for her constant support, guidance and encouragement throughout the last two years. I am grateful to her for the opportunity of working on this research project sponsored by Caterpillar, Inc.

I would like to convey special thanks to Dr. Jesse J. Brown, Jr. for his invaluable advice and assistance during this research and also for serving on my committee. I also wish to thank Dr. Ronald S. Gordon for serving on my committee. Thanks are also extended to Dr. Ran Datta for his helpful discussions and suggestions; Dr. Rajan Tandon of Caterpillar, Inc. for providing the silicon nitride samples; and Dr. Norman Eiss of the Mechanical Engineering Department, Virginia Tech, for his help in conducting the wear tests.

I would also like to thank Jan Doran, LeeAnn Ellis and Amy Hill for their kindness and help throughout my stay at the department.

I would like to take this opportunity to thank Judson Marte, Thierry Nguyen, Aprillya Rosidian, John Stuecker and Virginie Vaubert for their support and friendship.

Finally, I thank my husband, Raj, whose love and support have helped me through the good and bad times of the masters program and who has remained at my side through all.

Table of Contents

List of Illustrations

List of Tables

1.0 Introduction

In the early 1980s, with the manufacture of ceramic glow plugs, silicon nitride (Si_3N_4) ceramic material was first introduced commercially as a potential candidate for engine components.[1] Since then several kinds of Si_3N_4 reciprocating engine components such as swirl chambers, rocker arm pads, turbo-charger rotors, and exhaust control valves have been put into practical use.[1,2] Furthermore, the light weight and the excellent wear resistance properties of Si_3N_4 have proved to be very advantageous for its usage as various valve train components such as valve guides, valve spring retainers, pistons, and exhaust valves. The replacement of conventional valves made of steels, super alloys and titanium alloys by lighter weight Si_3N_4 ceramic valves has led to approximately 60% reduction in weight, which in turn has resulted in higher engine speed and horsepower.[3,4] Thus, Si_3N_4 which also possesses a combination of properties such as high hardness, chemical stability, ability to be ground with a very smooth surface to high tolerances and strength retention over a broad temperature range, has earned immense importance in various industrial engine applications.[3]

Although Si_3N_4 has the potential for use in certain high-performance applications, its commercialization has not occurred as rapidly as anticipated primarily due to high production costs. Machining of as processed Si_3N_4 constitutes a large proportion of production costs. It involves a rather complicated and expensive routine, especially when complex parts are manufactured. Surface flaws such as voids, produced as a consequence of processing, or pits, created by exposure to the environment, are commonly present on the as processed surfaces of Si_3N_4.[5] Si_3N_4 materials are very sensitive to surface flaws and to reduce the detrimental effect of such flaws, finishing and machining operations are required.[5,6]

In polycrystalline ceramics like Si_3N_4 subjected to external forces, fracture originates at surface flaws initiated in the as fired condition. The objective of this research is to develop a low expansion glaze coating on as fired Si_3N_4 in an attempt to enhance strength by reducing the effect of surface flaws and to offer an inexpensive alternative to machining. Preliminary work focused on the synthesis and characterization of two glaze compositions belonging to the lithia-alumina-silica (Li_2O-Al_2O_3-SiO_2) and magnesia-alumina-silica (MgO-Al_2O_3-SiO_2) systems. The glazes of these compositions can be formulated to possess lower coefficients of thermal expansion than the Si_3N_4 substrate. This ensures compressive residual stress on the surface, which may reduce the effects of surface flaws when the body is stressed.[7,8] The effect of glaze coatings on the room temperature flexural strength and failure mechanisms of as fired Si_3N_4 was investigated. Finally, the wear properties of the coated Si_3N_4 were examined to indicate how coatings may affect performance.

2.0 Review of Literature

2.1 Silicon Nitride

Silicon nitride structural ceramics were first developed in 1955 by Collins in the U.K.[8] But actual practical applications of Si_3N_4 started to progress in 1981 when the "Fine Ceramics Project" began in Japan and ceramic glow plugs made of Si_3N_4 were introduced into the commercial market for the first time. The "Fine Ceramics Project", a government sponsored project, in 1981-1992 contributed much to the acceleration in the development of Si_3N_4 ceramics.

Silicon nitride ceramics are lighter and have better wear and abrasion resistance than metals.[4,9-11] These features make them prime candidate materials for low temperature wear, as well as engine and hydraulic system applications. The lower density of Si_3N_4, compared to metals, reduces both weight and stresses created in moving components. The wear resistance of Si_3N_4 has been the key factor in improving wear rates and reducing friction in rocker arm pads made of Si_3N_4 as compared to those made of conventional sintered ferrous alloy pads as shown in Figure 2.1.[3]

The prospect of utilizing Si_3N_4 as an engineering material is dependent on its cost reduction. Machining of Si_3N_4 materials constitute a major proportion of production costs. Machining of as processed Si_3N_4 surfaces is required to meet dimensional tolerances, achieve improved surface finish, and remove surface flaws. Si_3N_4 ceramics are difficult and expensive to machine due to their high hardness and brittle nature. Thus, machining can represent a significant portion of the cost of fabrication and should be minimized as much as possible.[5,6]

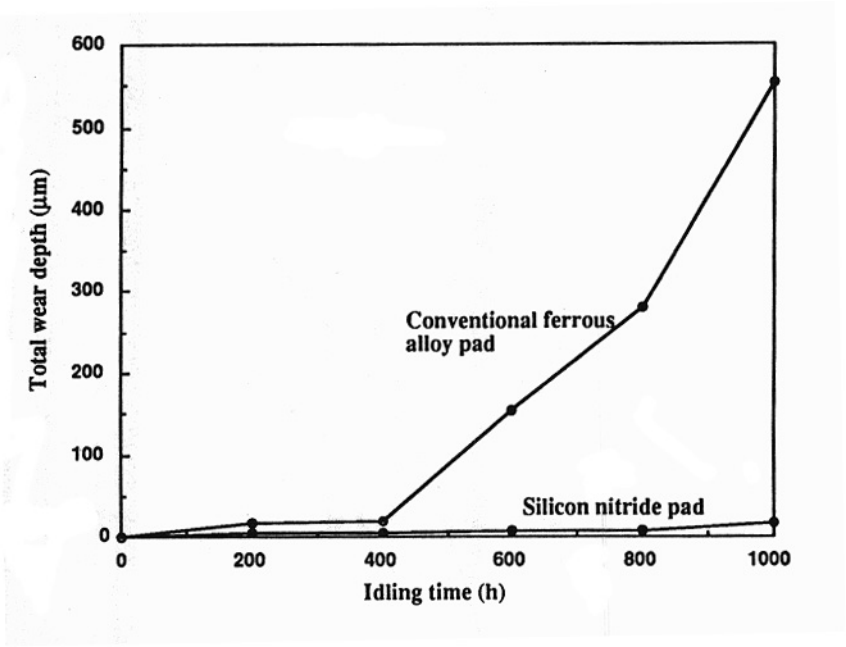

Figure 2.1 Comparison of the total wear depth of a conventional ferrous alloy pad versus a silicon nitride pad.[3]

2.2 Effects of surface flaws on fracture

The strength of brittle ceramics is a bulk property which is largely controlled by surface condition.[12,13] It is generally accepted that the mode I stress intensity, K_I, at the tip of a surface flaw of length c, under an applied tensile stress σ_a, is given by

$$K_I = \sigma_a \sqrt{\pi \Omega c}$$

where Ω is a geometric factor which depends on the shape of the flaw tip. Failure occurs when K_I exceeds the critical stress intensity K_{IC}. Thus, surface flaws act as stress concentrators, the stress at the flaw tip being much greater than if there were no flaws present. Because the actual geometry of the flaws can be very complicated and there is no means of studying flaw shapes, it is reasonable to consider the likely effect of variations in flaw size and shape in terms of simple geometries.[14]

It is generally known from fracture mechanics that, under an applied stress, a surface flaw will have a higher stress intensity than a volume flaw at the same stress.[15] This fact is clearly demonstrated by as-received 99% pressure-sintered alumina rods, which had an initial strength of 388 MPa, showed a strength of 722 MPa when the presence of compressive surface layer shifted the fracture origins so that fracture occurred at volume flaws rather than at surface flaws.[16] Thus, the location of defects is of critical importance to designers because surface located defects behave very differently than identical flaws located in the bulk.[15] Figure 2.2[15] shows a schematic of surface flaw and volume flaw in a ceramic.

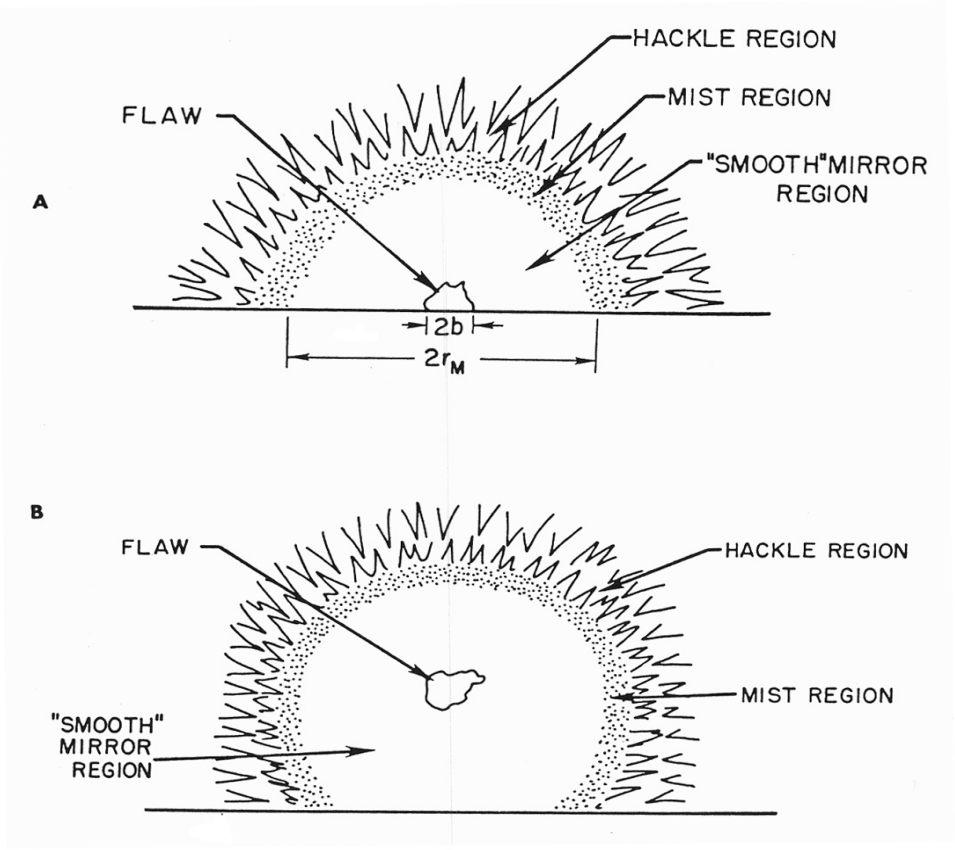

Figure 2.2 Schematic of the fracture surface of an advanced ceramic which failed in a brittle manner showing a defect at the surface (A) and in the volume (B) and the intrinsic fracture markings.[15]

2.3 Strengthening by compressive surface stress

Development of compressive surface layers on the as fired Si_3N_4 surface can eliminate or minimize the effect of surface flaws and can be an attractive alternative to machining. Compressive surface stresses have been used to strengthen ceramics since very ancient times. Most pottery and chinaware are strengthened due to the creation of compressive surface stresses by the application of low expansion glazes.[7] The formation of compressive stress on the surface raises the nominal stress at which the surface flaws can act to cause failure, thus improving the strength of the material. Materials of this type are called pre-stressed. In applying a force to the pre-stressed specimen, the compressive forces set up on the exterior surface of the specimen must first be overcome. The added strength is due to this factor, for in a pure body, the specimen would immediately be subjected to tension with no resisting forces to overcome.[17]

The relative thickness of the compressive surface layer gives rise to differences in the stress profiles. The distributions of stresses through the thickness of a pre-stressed material are illustrated in Figures 2.3(A), (B) and (C).[7] Effects of applied flexural and tensile loads on the stress profiles are indicated. Under no load, thin compressive surface layers give rise to low and almost constant tensile stresses in the interior of the body (Figures 2.3(A) and (B)) while the stress distribution is approximately parabolic when the surface compression layer is considerably greater than the depth of the most severe flaw (Figure 2.3 (C)).[7,14] Thus, thicker compressive layers give rise to greater residual tensile stresses in the interior.

The most common example of surface compression is in safety glass. Surface compression is achieved in glass most commonly by either ion exchange or quenching. In the former case, the glass is exposed at elevated temperature to positive ions that are larger than those initially in the glass. Since the glass structure is expanded at the elevated temperature, these larger ions are able to trade places with the smaller ions near the surface. When the glass is cooled, these ions no longer fit, but are trapped in the structure and result in surface compression.[8] Surface compressive layer due to ion exchange has also been produced in fine-

grained glass-ceramics containing a large proportion of β-spodumene solid solution crystals by immersion in molten sodium and potassium salt baths which placed sodium and potassium ions in lithium sites in the β-spodumene structure.[18] On the other hand, improving strength by quenching has been known for a long time. Quenching was used to strengthen alumina (Al_2O_3), titania (TiO_2), spinel ($MgAl_2O_4$), steatite ($MgSiO_3$), forsterite (Mg_2SiO_4), and silicon carbide (SiC). Quenching Al_2O_3 rods from 1600°C into silicone oil resulted in an increase in the average strength from 331 MPa to 694 MPa.[7,19] For quenching to be effective, the material must be heated to a temperature such that some plasticity is present. A temperature of 1500 to 1600°C is appropriate for Al_2O_3, but 1900 to 2000°C is required for SiC. During quenching the surface cools very rapidly and is placed in compression as the interior cools relatively slowly.

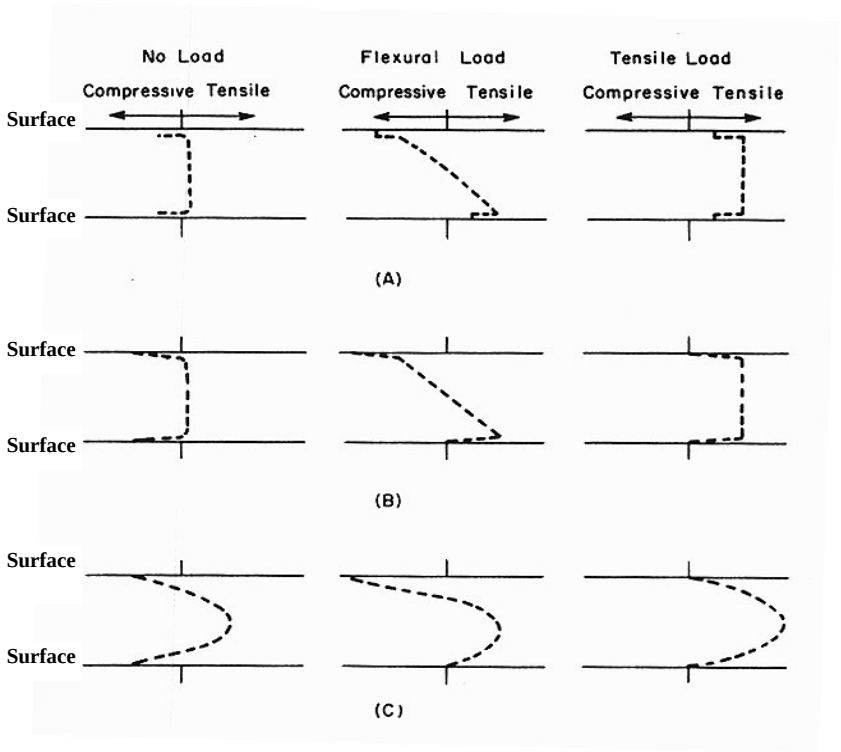

Figure 2.3 Schematic stress profiles in a pre-stressed material with (A) thin compressive surface layer. (B) diffused surface layer. (C) thick surface layer.[7]

Chemical methods have been widely used to strengthen glasses. The use of these methods was extended to glass-ceramics, conventional polycrystalline ceramics, and oxide single crystals. Compressive surface layers were developed by chemical strengthening process through the formation of low expansion solid solution surface layers on oxide ceramics. Low expansion solid solution surface layers were applied to polycrystalline ceramics at high temperature which allowed the main body to contract more than the surface layers during cooling at room temperature, placing the surface layers in compression. This approach was successfully applied to Al_2O_3 - Cr_2O_3 solid solution - alumina; MgO•Cr2O3 - MgO•Al_2O_3 solid solution - spinel; TiO_2 - SnO_2 solid solution - titania; and MgO - NiO solid solution - magnesia combinations.[16,19] The Al_2O_3 - Cr_2O_3 solid solution surface layers were also effective in strengthening sapphire single crystals.[20] Low expansion solid surface layers were used to increase the strength of magnesia single crystals.[21]

2.4 Glazes

Glazes are vitreous coatings, usually prepared from fused silicate mixtures fusion-bonded to ceramic surfaces.[23] Like glasses, they are not definite chemical compounds but complex mixtures which sometimes are described as "undercooled solutions." Glazes are commonly applied on clay wares and other ceramics for many reasons. They may serve as protective coatings to increase strength, to make the substrates chemically more inert, more readily cleanable and to provide an aesthetically attractive coating which covers up blemishes and provides a decorative effect.[24]

There are three principal components in a glaze composition:

(i) Acids, which are represented by the RO_2 classification, of which SiO_2, SnO_2, ZrO_2, TiO_2, CeO_2, and ThO_2,are the common examples.

(ii) Bases or the fluxing agents, which are of the form represented by the RO and R_2O classification per the ceramic nomenclature, include mainly the alkalies and the alkaline earths such as Li_2O, Na_2O, K_2O, BeO, MgO, CaO, BaO, SrO, PbO, ZnO, FeO, MnO, CdO, CuO, NiO and CoO.

(iii) Intermediates, which include the amphoteric oxides, represented by R_2O_3 classification of which Al_2O_3, B_2O_3, Fe_2O_3, Cr_2O_3, Bi_2O_3 are the common examples.

Among the acids, silica (SiO_2) - the glass former - is an essential glaze ingredient. This single material would suffice to form a glaze, were it not for the fact that the melting point of the SiO_2 is so high - about 1700°C. Thus to lower the melting point and also to increase the fluidity of the glaze, bases or fluxing agents must be added to the glaze composition. The kind and the content of the bases used in a glaze have a direct bearing upon its thermal expansion properties. Lastly, the intermediates or the amphoteric oxides are also required in a glaze composition, because they give added hardness and toughness to the glaze, allow a higher maturing temperature, increase viscosity, and prevent devitrification. Alumina (Al_2O_3) is the most commonly used amphoteric oxide in a glaze which acts as a refractory element and helps to form a stronger glaze that can better withstand the wear of normal use.[23,25]

Glazes can be manufactured in two distinct ways. They can be prepared from materials insoluble in water which are ground and mixed with water to produce glaze slips. This type of glazes are known as raw glazes which are applied on to the substrate surface and are then matured by firing the glazed specimen. An alternative way to constitute a glaze is to first prepare a pre-melted, glassy frit which is manufactured from melting usually water soluble materials followed by its subsequent quenching in water. The glaze is then made from grinding and mixing the glassy frit with water to produce the glaze slip. This kind of glazes is known as fritted glazes. The advantage of using fritted glazes as compared to raw glazes is better maturing, more uniformity, and fewer defects due to the elimination of a large portion of the evolved gases. Work to date has shown that if a glaze is first formed as a frit, it yields good results for a twice-

fire procedure where the glaze is applied to an already fired body and the second firing cycle matures the glaze.[25,26]

2.5 Strengthening by glazing

Glazes, after being applied to ceramic bodies, need to be fired to achieve fusion of the coating with the substrate. Then, when the fired ceramic ware is cooled, the whole coated substrate undergoes contraction. If the coefficients of thermal expansion (CTE) of the coating and the substrate are not sufficiently close together, stresses and strains are set up due to thermal expansion mismatch at the coating/substrate interface, resulting in defects such as spalling or crazing. Although the CTE of the coating and the substrate need to be close, they usually are not identical. Because ceramic coatings and ceramic bodies are much stronger in compression than in tension, the weaker of the coating-substrate combination, namely, the coating, must be put in compression. In order to achieve this, a coating must be selected with a coefficient of thermal expansion somewhat lower than that of the substrate. Thus, when the coated body is cooled after firing to a certain temperature, the coating shrinks less than the substrate and is therefore compressed. The direction of the compressive stress in the glaze will be parallel to the surface of the substrate. Any tensile stresses applied to the substrate would first need to neutralize the existing surface compressive stress before acting on any flaws to cause failure. As the extent of any compressive stress is limited to the thickness of the glaze, no flaws should exist which are greater than the thickness of the glaze. Normally, glazes with thickness greater than 50μm are applied on glass containers, because the critical flaw size in typical commercial glassware is known to be about 20μm.[14]

The method of strengthening materials by glazing has been used previously which led to the development of surface compressive stresses. Low expansion zinc borate glazes were applied to the surfaces of glass containers using flame spraying process.[27] When the containers were pressure tested it was found that the bursting strengths of the containers were significantly

increased. Another technique for inducing compressive surface layers used glazing followed by quenching. Surface compression was obtained in polycrystalline alumina when a glaze, with a coefficient of thermal expansion of 5.3 x 10^{-6} $°C^{-1}$ was applied on Al_2O_3, which has a coefficient of thermal expansion of 6.5 x 10^{-6} $°C^{-1}$.[16,28] The specimen was fired to a temperature much higher than the normal maturing temperature of the glaze and was then quenched by removing the hot specimen from the furnace and cooled rapidly in an air blast. Quenching was also done by dipping the specimen in motor oil, silicone oil, or water. Thus, a strength of 767 MPa was obtained for Al_2O_3 that was glazed and quenched, compared to 331 MPa for as-received material. Glazing followed by quenching, was also utilized to form compressive surface layers on sapphire rods.[20] In this case, however, the average flexural strength value obtained for glazed and slow cooled sapphire specimens was very similar to that for glazed and quenched specimens.

2.6 Low expansion glazes

Low expansion glazes have been used to strengthen ceramics since antiquity.[7] Glazes with very low expansion can be formulated within the Li_2O-Al_2O_3-SiO_2 system from which β-spodumene ($Li_2O{\bullet}Al_2O_3{\bullet}4SiO_2$) and/or β-eucryphite ($Li_2O{\bullet}Al_2O_3{\bullet}2SiO_2$) phases crystallize during firing.[29] Very low thermal expansion glazes can also be formulated from compositions which develop crystals of cordierite ($2MgO{\bullet}2Al_2O_3{\bullet}5SiO_2$) on firing.[25,26] This type of glaze can be applied on cordierite ceramics (ceramics having a substantial content of cordierite crystals) or any other low expansion ceramic bodies. Being of low expansion themselves, cordierite ceramics require glazes of very low expansion. Very few glazes are known which have expansions lower than cordierite ceramics. Self-glazing techniques are known for cordierite bodies, wherein a glaze "skin" self-forms on the body during firing of the body itself, without application of a separate glaze.[26] However, it is difficult to control the physical properties of self-glazed cordierites. Eppler and O'Conor[29,30] formulated a glaze composition, suitable for application on cordierite bodies, by precipitating a low expansion phase within the Li_2O-Al_2O_3-SiO_2 system. Prall[26] developed a cordierite crystal-containing glaze for fine ceramics such as cordierite from

compositions within the $MgO-Al_2O_3-SiO_2$ system. Thus, the two main ternary systems from which low expansion glazes can be formulated are $Li_2O-Al_2O_3-SiO_2$ and $MgO-Al_2O_3-SiO_2$.[25,26,30]

2.6.1 Lithia - Alumina - Silica

Glass ceramics exhibiting very low coefficients of thermal expansion are made by choosing compositions in the $Li_2O-Al_2O_3-SiO_2$ system.[14,31] In the $Li_2O-Al_2O_3-SiO_2$ ternary system, the region of glasses is not large, but passes through the region of minerals with a low or negative coefficient of thermal expansion as shown in Figure 2.4.[32] Regions I and II in the figure correspond to regions of negative thermal expansion. Three compositions, within these two regions and along the $Li_2O.Al_2O_3.SiO_2$ join, are naturally occurring minerals spodumene, petalite and eucryptite.[33,34] The lithia to alumina ratio is constant for each of the three minerals while the silica contents varies in each of them. Remarkably low expansion coefficients are exhibited by the β forms of the minerals. As shown in Figure 2.5[34], these vary from slightly positive, for β-spodumene, to highly negative, for β-eucryptite. Eucryptite ($Li_2O.Al_2O_3.2SiO_2$) and spodumene ($Li_2O.Al_2O_3.4SiO_2$) undergo fast crystallization at 500°C and 700°C respectively.[35]

Hummel[34,36] reported the unusually low thermal expansion coefficient of β-spodumene, synthesized from commercially available α-spodumene. The thermal expansion of α-spodumene was found to be 4×10^{-6} °C^{-1} up to about 900°C, when it transformed to β-spodumene with a linear expansion of 1.9×10^{-6} °C^{-1}. On firing β-spodumene between 1100° - 1200°C, the thermal expansion increased to 2.4×10^{-6} °C^{-1} due to the formation of glassy phase. The thermal expansion coefficient of calcined commercial petalite, or β-spodumene solid solution, was reported by Hummel to be about the same as or slightly lower than that of fused silica, which has a thermal expansion coefficient of 0.5×10^{-6} °C^{-1}. Hummel also reported the thermal expansion coefficient of the naturally occurring mineral, α-eucryptite to be of -0.64×10^{-6} °C^{-1}. α-eucryptite inverts to a high temperature form, β-eucryptite at around 900°C which also has a negative thermal expansion coefficient.

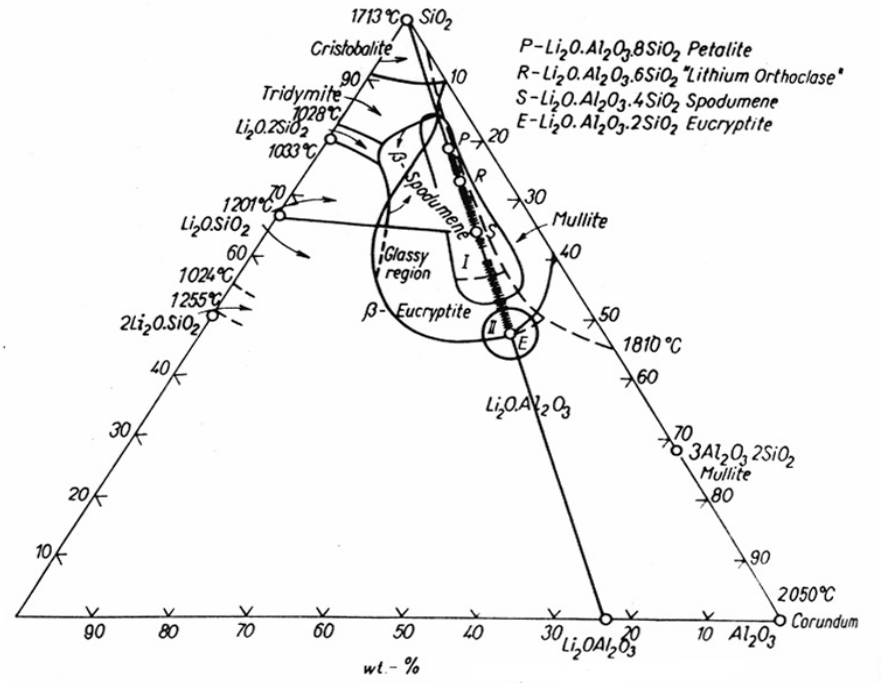

Figure 2.4 Phase diagram for the Li_2O-Al_2O_3-SiO_2 system[32]

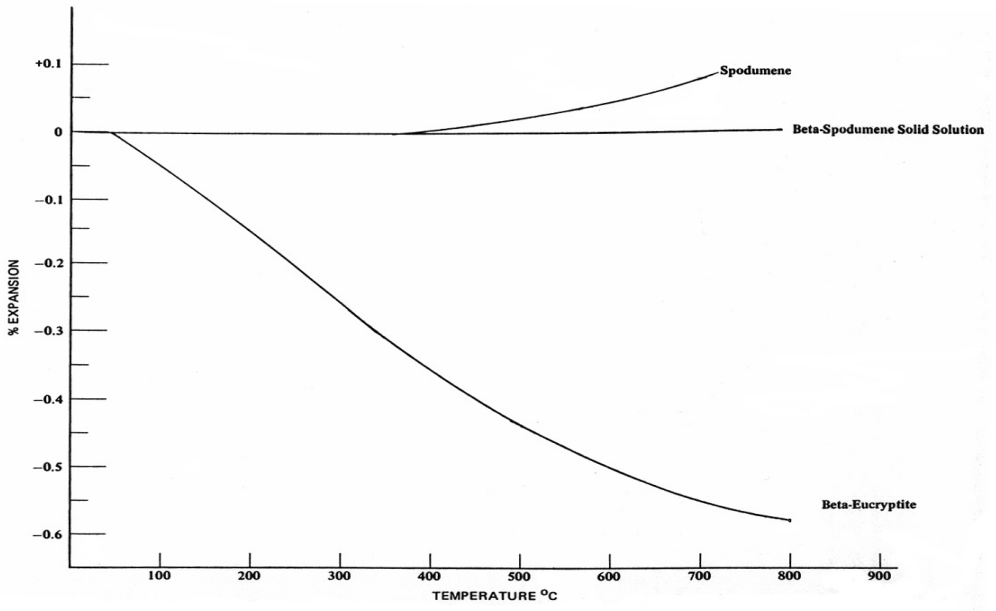

Figure 2.5 Thermal expansion curves for β-spodumene and β-eucryptite[34]

2.6.2 Magnesia - Alumina - Silica

Glass ceramics in the $MgO\text{-}Al_2O_3\text{-}SiO_2$ system are mainly represented by cordierite ($2MgO.2Al_2O_3.5SiO_2$). Cordierite is a crystalline substance with a low thermal expansion coefficient. Besides cordierite, mullite ($3Al_2O_3.2SiO_2$) and spinel ($MgO.Al_2O_3$) and other crystalline phases may also precipitate as shown in the ternary diagram, Figure 2.6.[37] In the phase diagram, the region of primary crystallization of cordierite corresponds approximately to the proportion of components in the ranges of 45-60 wt.% SiO_2, 20-30 wt.% Al_2O_3 and 2-18 wt.% MgO.[37]

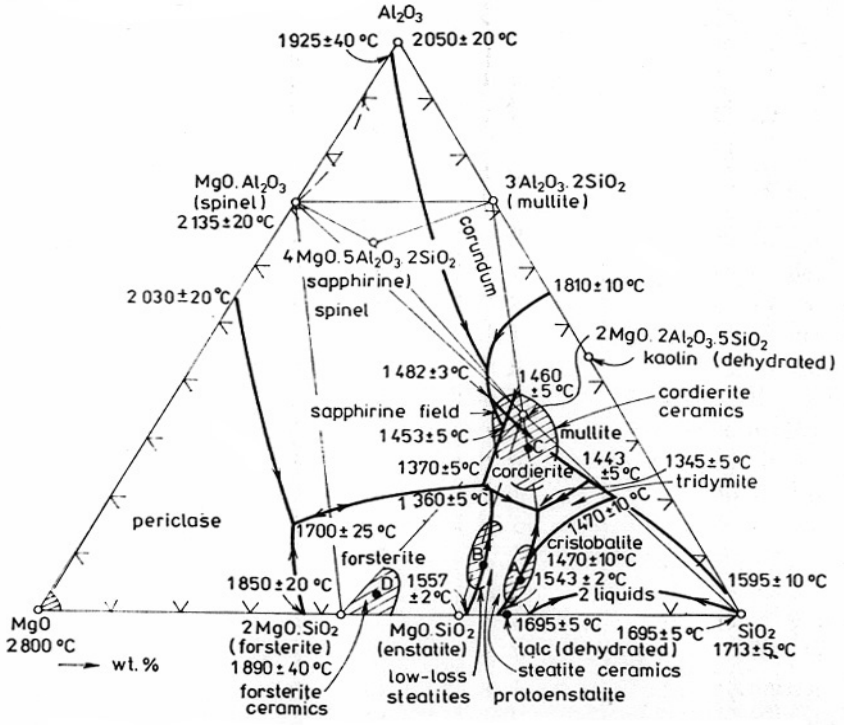

Figure 2.6 Phase diagram for the $MgO\text{-}Al_2O_3\text{-}SiO_2$ system[37]

Three polymorphic forms of cordierite have been reported, two stable (β,α) and one metastable form (μ).[38] The high temperature α form develops from solid state reactions of batch

materials and from the devitrification of glass between 1050 and 1460°C. The metastable μ form can be obtained by heating powdered glass for many hours at 800 to 900°C. The β and μ phases invert to the α form in the range above 830°C. Hummel[38] measured the coefficient of thermal expansion of μ cordierite as 4.7 x 10^{-6} $°C^{-1}$ and the α form as 2.5 x 10^{-6} $°C^{-1}$ for the range 25° to 1000°C. Temperatures in excess of 1500°C are necessary for melting components which give rise to cordierite ceramics and the melts have comparatively low viscosity.[37] Because cordierite ceramics have the disadvantage of difficult melting and also a high crystallization temperature (1000°C), they have found less practical application than glass-ceramics of the spodumene type.[32] However, after crystallization, they exhibit a high strength (up to 250 MPa in bending), a high electrical resistivity and low dielectric losses, and are used in applications such as electrical insulators and high-frequency electrotechnical materials.[37,39]

3.0 Experimental Procedure

This chapter discusses the various experimental steps that were undertaken to accomplish the research objectives. The steps involved were: (i) glaze formulation which consisted of frit preparation followed by glaze preparation, (ii) surface cleaning and pre-treatment of Si_3N_4, (iii) glaze application, (iv) room temperature flexural strength evaluation, and finally, (v) wear tests.

3.1 Glaze Formulation

3.1.1 Preparation of frit and glaze of composition A

To prepare the frit, raw materials (source: Fisher, Aldrich) were used and weighed out in proportions as shown in Table 3.1. This composition was chosen to formulate a low expansion glaze which was originally developed for application on low expansion ceramics like cordierite.[30] Hot pressed Si_3N_4, similar to cordierite, exhibits a CTE of 3.2 x 10^{-6} °C^{-1}.[40]

Raw material and formula	Batch wt. (gms.)
Potassium Nitrate [KNO_3]	6.3
Boric Acid [$B_2O_3.3H_2O$]	2.7
Lithium Carbonate [Li_2CO_3]	5.9
Zircon [$ZrSiO_4$]	26.7
Alumina [Al_2O_3]	2.7
Spodumene [$Li_2O.\ Al_2O_3.\ SiO_2$]	55.6

Table 3.1 Batch composition of frit A

The oxide composition of the frit is shown in Table 3.2. The different raw materials were dry mixed using mortar and pestle for 15 minutes and the batch was then heated at the rate of 1.5°C/min for the first 1000°C to allow the effluent gases to escape from the frit batch. The slow heating up to 1000°C gave enough time for the boric acid to lose its water of crystallization, because complete dehydration of boric acid occurs at around 1000°C.[32]. The batch was finally heated to 1400°C at 1.5°C/min and held at that temperature for 1 hour. The molten batch was then taken out of the furnace and quenched in water to form glass frit. The frit was dried and ball-milled, using Al_2O_3 milling balls, under dry conditions for 16 hours. Subsequently, 100 parts (44.53g) of dry-milled frit, 4 parts (1.78g) bentonite clay and 45 parts (22.03ml) water were mixed and ball-milled for 1 hour. The bentonite (source: Fisher), which is a colloidal material and is a type of clay, was used as a suspending agent that helped prevent settling in the glaze and improve glaze application. The glaze slip was then passed through a 325 mesh sieve to remove undesirable coarse fragments. Finally, the slip was adjusted to a viscosity between 200 and 300 cP

Oxide composition	**wt.%**
SiO_2	55.1
Al_2O_3	13.0
Li_2O	17.0
ZrO_2	10.8
K_2O	2.5
B_2O_3	1.6

Table 3.2 Oxide composition of frit A

by adding water. The composition of the glaze (Table 3.3) had to be adjusted slightly from that of

Oxide composition	**wt%**
SiO_2	55.4
Al_2O_3	13.0
Li_2O	16.7
ZrO_2	10.6
K_2O	2.5
B_2O_3	1.6

Table 3.3 Oxide composition of glaze A

the frit after bentonite addition. The composition of the bentonite clay per the chemical datasheet is shown in Table 3.4.

Oxide composition	wt.%
SiO_2	73
Al_2O_3	14
MgO	1.1
Na_2O	0.6
K_2O	1.9
CaO	0.2
Fe_2O_3	2.7

Table 3.4 Chemical composition of bentonite clay

3.1.2 Preparation of frit and glaze of composition B

To prepare the frit, the batch materials (source: Fisher, Aldrich) were weighed as shown in Table 3.5. The batch composition was chosen to develop a low expansion cordierite crystal-containing glaze.[26] Table 3.6 shows the oxide composition of the frit. The weighed batch was dry mixed using mortar and pestle for 15 minutes and placed in the furnace for melting. The batch was heated at the rate of 2°C/min to 1000°C and then fired to 1600°C at the rate of 5°C/min. This was done to allow enough time for the elimination of the gases evolved from the

Material and formula	wt. in g
Silica [SiO_2]	72.0
Alumina [Al_2O_3]	15.2
Magnesia [MgO]	7.1
Boric Acid [$B_2O_3.3H_2O$]	3.9
Sodium Carbonate [Na_2CO_3]	0.8
Potassium Carbonate [K_2CO_3]	0.2
Calcium Carbonate [$CaCO_3$]	0.5
Zirconia [ZrO_2]	0.3
Ferric Oxide [Fe_2O_3]	0.2

Table 3.5 Batch composition of frit B

carbonate compounds in the frit batch. This also insured that all of the water was lost from the boric acid in the batch. The batch was kept at 1600°C for 4 hours, after which the molten batch was taken out of the furnace and poured into water to frit it. The frit was then dried and ball-milled for 16 hours. Weight of the resulting powdered dry frit was measured to be 28.51g. Subsequently, 4 parts bentonite (1.14g) and 45 parts water (12.83ml) were added to 100 parts of the powdered frit and ball-milled together for 1 hour. Bentonite was used to act as a suspending agent. The glaze slip, thus prepared, was then passed through a 325 mesh sieve to remove undesirable coarse fragments. The slip, with particle size -325 mesh, was then adjusted to a viscosity between 200 and 300 cP by adding water.

Oxide composition	**wt. %**
SiO_2	73.6
Al_2O_3	14.9
MgO	7.3
B_2O_3	2.3
Na_2O	0.6
K_2O	0.2
CaO	0.4
ZrO_2	0.4
Fe_2O_3	0.3

Table 3.6 Oxide composition of frit B

With the addition of 4 parts bentonite, the composition of the glaze slip became slightly different from that of the frit batch. The composition of the bentonite clay per the chemical datasheet is shown previously in Table 3.4. The composition of the glaze was calculated and is shown in Table 3.7.

Oxide composition	wt.%
SiO_2	73.6
Al_2O_3	14.9
MgO	7.2
B_2O_3	2.2
Na_2O	0.6
K_2O	0.2
CaO	0.4
ZrO_2	0.4
Fe_2O_3	0.3

Table 3.7 Oxide composition of glaze B

3.2 Surface cleaning and pre-treatment of Si_3N_4

Hot pressed Si_3N_4 specimens with sintering additives Y_2O_3 and Al_2O_3 were obtained from Caterpillar, Inc. To remove possible contaminants, as processed Si_3N_4 samples were ultrasonicated in acetone for 1 hour. The samples were then further cleaned by soaking them in deionized water and ultrasonicating for another hour. Subsequently, the specimens were dried at 110°C for 2 hours.

In some Si_3N_4 specimens, after surface cleaning by ultrasonicating in acetone for 1 hour and drying at 110°C for 2 hours, surface pre-treatment was accomplished by immersing the specimens in a 20% HF solution for 5 minutes. Next, the samples were washed with deionized water, dried at 110°C for 2 hours and calcined in air at 1200°C for 6 hours. Finally, the specimens were kept in a 10% HCl solution for 10 minutes, then rinsed with deionized water and dried at 110°C for 2 hours.[41]

3.3 Glaze Application

3.3.1 Glaze A coating

The glaze of composition A was applied on the as processed surfaces of Si_3N_4 by brushing a thin coat, which was allowed to dry for 4 hours. Another thin coat was applied on top of the first coating and was allowed to dry at room temperature for 24 hours. Care was taken to apply the glaze in such a way as to give a total uniform smooth coverage with few irregularities such as ripples or runs in the coating as possible. To achieve crystallization of the glaze and to reduce crack formation, the specimens were fired according to a step controlled heating-cooling procedure. The heat treatment schedule for glaze A coating is shown in Figure 3.1. This schedule proved to be the optimum one after trying several variations with different heating rates and intermediate hold times. The maximum firing temperature in the schedule was fixed at 1130°C.[30] Faster heating rates resulted into formation of cracks and blisters in the coating.

3.3.2 Glaze A + Na_2SiO_3 coating

The glaze A coated Si_3N_4 specimens did not develop a very smooth surface. To achieve greater surface smoothness, a modification to the above coating procedure was attempted. A powder mixture of 10g Na_2CO_3 and 5.64g SiO_2 (equivalent to Na_2O : SiO_2 = 1 : 1 molar ratio) was heated at 1000°C for 24 hours to form Na_2SiO_3. According to the phase diagram, shown in Figure 3.2[42], Na_2SiO_3 forms and remains as a stable phase up to about 1075°C when equimolar ratio of Na_2O and SiO_2 are heated together. The synthesized Na_2SiO_3 powder was mixed with 10ml of water to form Na_2SiO_3 solution. After applying a thin layer of Na_2SiO_3 solution on the already fired glaze A coated specimen, the specimen was fired according to the heating schedule as shown in Figure 3.3. The maximum firing temperature was fixed at 1100°C because according to the phase diagram, Na_2SiO_3 remains in the liquid phase above 1075°C. The heating rates and the hold times were kept identical to that of glaze A coating.

Room temperature

↓ 0.5°C/ min

700°C for 30 min

↓ 1.5°C/ min

1130°C for 1 h

↓ 1.5°C/ min

700°C for 30 min

↓ furnace cooled

Room temperature

Figure 3.1 Heat treatment schedule for glaze A coated specimens

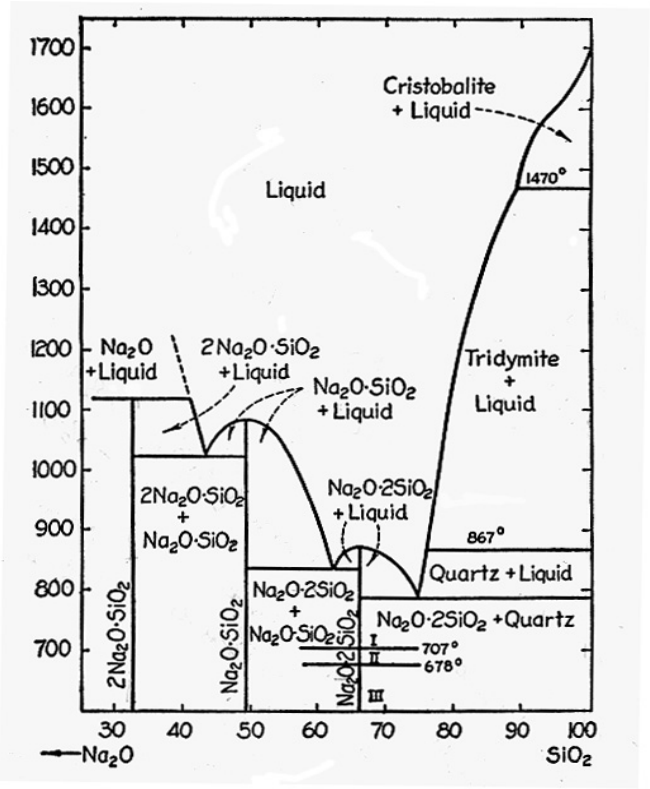

Figure 3.2 Phase diagram for the Na_2O-SiO_2 system[42]

Room temperature

↓ 0.5°C/ min

700°C for 30 min

↓ 1°C/ min

1100°C for 1 h

↓ 1°C/ min

700°C for 30 min

↓ furnace cooled

Room temperature

Figure 3.3 Heat treatment schedule for glaze A + Na_2SiO_3 coated specimens

3.3.3 Glaze B coating

A thin coating of the glaze of composition B was painted on to the as processed surfaces of Si_3N_4 specimens. The first coating was allowed to dry at room temperature for 4 hours. A second coating was applied on top of the first carefully to cover the substrate surface uniformly. After complete drying of the coating at room temperature for 24 hours, the specimens were fired following a controlled heating-cooling schedule as shown in Figure 3.4. After several trial runs, this heating schedule was chosen as the optimum one to achieve crystallization of the low expansion cordierite phase in the glaze and also to reduce crack formation. Attempts to fire with faster heating rates resulted into formation of cracks and blisters in the coating. The maximum firing temperature was fixed at 1330°C.[26]

The glaze coated specimens were characterized using SEM (scanning electron microscopy, model ISI SX-40, electron accelerating voltage 20kV), EDX (X-ray energy dispersive spectroscopy, model ISI SX-40, beryllium window) and XRD (X-ray diffraction analysis, International Scientific Instrument, model SX-40).

Room temperature

↓ 0.5°C/ min

700°C for 30 min

↓ 1°C/ min

1000°C for 15 min

↓ 1°C/ min

1330°C for 2.5 h

↓ 1°C/ min

700°C for 30 min

↓ furnace cooled

Room temperature

Figure 3.4 Heat treatment schedule for glaze B coated specimens

3.4 Room temperature flexural strength evaluation

3.4.1 Four-point flexural tests

The effect of glaze coatings on the strength of as fabricated Si_3N_4 specimens was examined by four-point bend test using Instron model 4204 testing machine. Room temperature tests were performed on 3 x 4 x 45 mm uncoated and coated MOR bars using crosshead speeds of 0.5 mm/min with inner and outer spans of 20 mm and 40 mm, respectively.

After the four-point bend testing, fracture surfaces of the broken specimens were analyzed using SEM to determine the failure mechanisms of uncoated and coated Si_3N_4 specimens.

3.5 Wear tests

Ball-on-flat wear tests were performed using a reciprocating wear apparatus (located in the Tribology Laboratory, Mechanical Engineering Department, Virginia Tech). The schematic of the apparatus is shown in Figure 3.4. The test materials were 3 mm diameter AISI 52100 steel balls, and uncoated and coated Si_3N_4 specimens with dimensions of 3 x 4 x 15 mm. The ball was mounted on to a 20 mm long steel cylinder. The test specimens were cleaned with acetone in an ultrasonic cleaner for 15 min, then rinsed with deionized water and dried at 110°C for 2 hours. Wear tests were conducted in air at room temperature and at a relative humidity of $50 \pm 5\%$.

In the wear test appraratus, the steel ball mounted on to the cylinder was held in a pivoted assembly which could not move along the horizontal direction. This was loaded with a 9.8 N weight. The Si_3N_4 flat specimens were secured with set screws on to a movable platform capable of oscillating in a to-and-fro motion with a peak-to-peak amplitude of 6.2 mm at a velocity of

8 mm/s against the fixed steel ball. This operation was performed under dry conditions without any lubricant. The total duration of each test was 1 hour. The friction force for each test was measured 30 min after the starting time of the experiment. After the tests, estimates of the damage were obtained from determinations of wear volumes using a surface profiler (Tencor Alpha-step 500 profiler) with 12.5μm radius stylus. Finally, the wear surfaces of the test specimens - steel balls and the uncoated and coated Si_3N_4 flats - were examined using scanning electron microscopy.

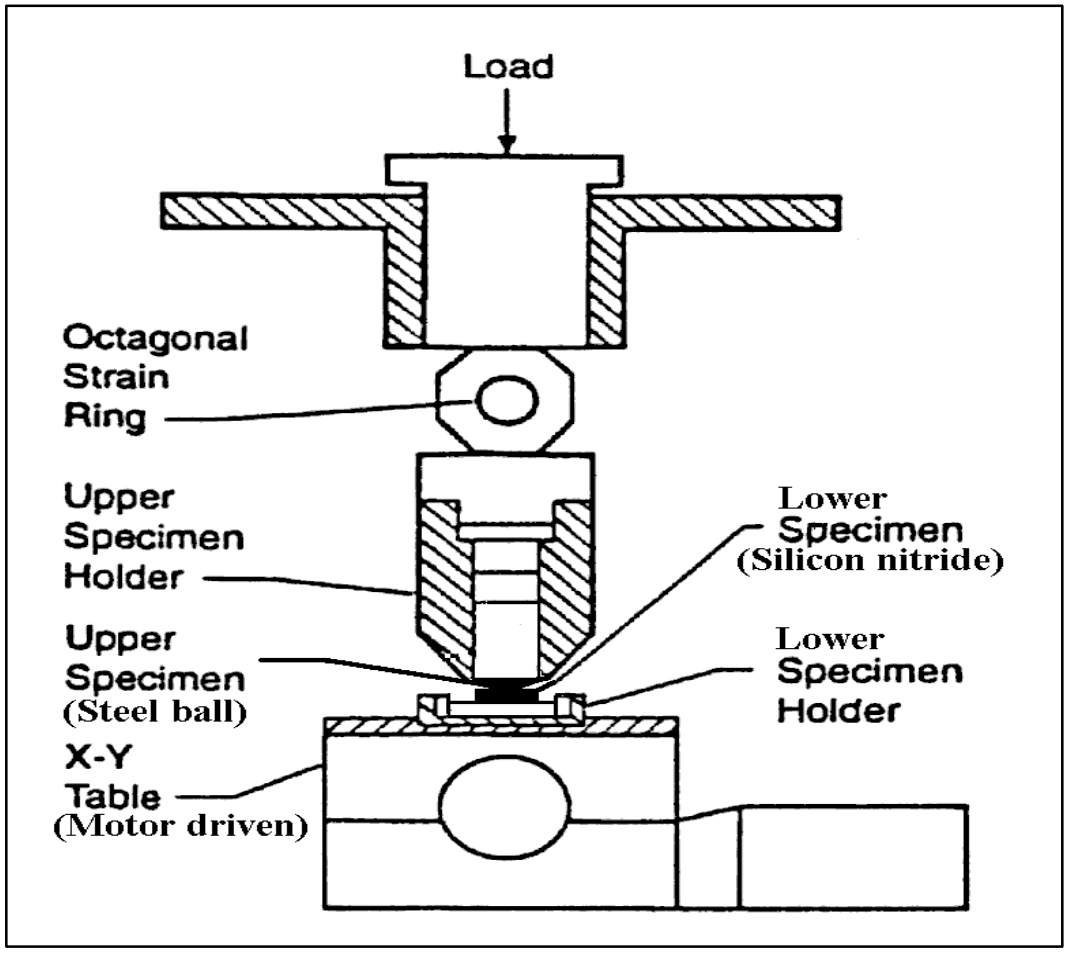

Figure 3.5 Schematic of the ball-on-flat sliding wear test apparatus

4.0 Results and Discussion

4.1 Surface pre-treatment of Si_3N_4

Surface pre-treatment was done on several as received Si_3N_4 specimens to determine if it helped the glaze coatings to achieve uniform spreading and good wetting on the substrate surface. However, based on SEM analyses it was found that surface treated and non-surface treated Si_3N_4 specimens exhibited the same coating characteristics, having identical microstructure and grain size. Because surface treatment did not enhance the adherence of the coatings to the substrate, surface pretreatment of as received Si_3N_4 specimens were not believed necessary or any of the subsequent experiments.

4.2 Glaze coating characterization

4.2.1 Glaze A coating

Homogeneous, crack-free, opaque and semi-crystalline glaze coatings of composition A were successfully formed on the as fired Si_3N_4 substrate. An SEM micrograph of the uncoated as fired Si_3N_4 surface is shown in Figure 4.1. The corresponding EDX elemental maps show the presence of Si, O, Al and Y. The elements Al and Y are detected due to the presence of sintering additives - Al_2O_3 and Y_2O_3 - used for hot pressing Si_3N_4. Figure 4.2 shows the SEM micrograph of the glaze A coating on the as fired surface of Si_3N_4. The corresponding EDX analyses revealed the presence of Si, O, Al, Zr, and K elements. The element Li, a major constituent of the glaze composition, could not be mapped because EDX was not able to detect a light element such as Li. The presence of Zr and K elements confirmed the coverage of the Si_3N_4 surface by the coating.

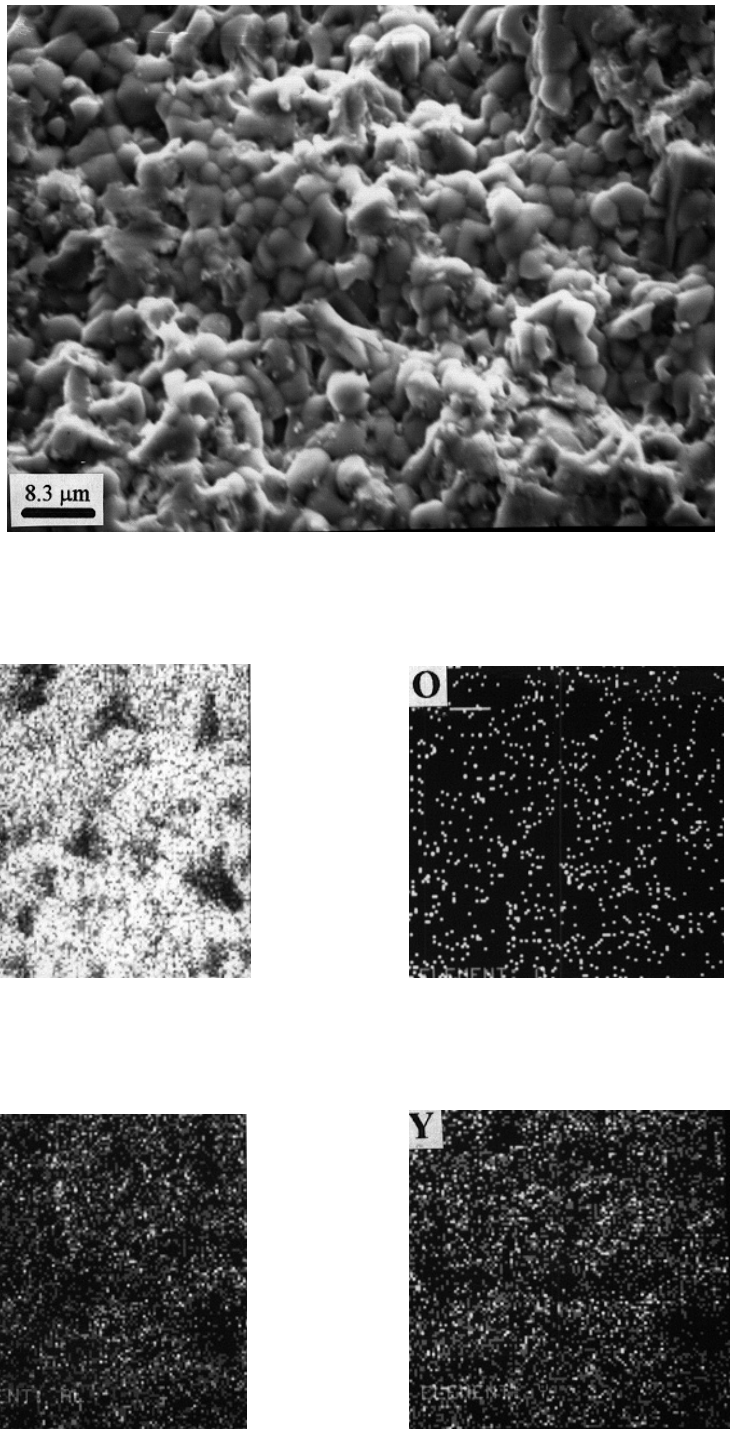

Figure 4.1 SEM micrograph and elemental mappings of uncoated as fired Si_3N_4

The EDX elemental mappings also revealed the higher concentration of element Zr on the 1-3μm size spheroidal grains present on the glazed surface. The elements Si, Al, O and K were uniformly distributed over the entire coated surface. Figures 4.1 and 4.2, both at 1200x magnification, indicate that the glaze formed a uniform coating on the Si_3N_4 substrate filling in the voids or pits present on the as fired surface. By comparing the SEM micrographs (Figures 4.1 and 4.2), it is noted that the glaze coating helped increase the smoothness of the as fired Si_3N_4 surface. For developing a crack-free uniform coating, the viscosity of the glaze slip had to be adjusted between 200-300 cP before being applied on to the substrate. It was found that if the viscosity of the glaze slip was below 200 cP, the coating became too thin and runny, and did not adhere to the substrate surface very well leaving behind unglazed regions on the surface. On the other hand, if the viscosity was higher than 300 cP, the coating became too thick and inhomogeneous. Figures 4.3 and 4.4 show the EDX spectra corresponding to entire surfaces of uncoated and coated Si_3N_4. The peaks of Zr and K in the EDX spectrum, shown in Figure 4.4, again confirmed the presence of glaze A coating covering the entire Si_3N_4 substrate. Figure 4.5 shows the X-ray diffraction pattern for the glaze A coated Si_3N_4 specimen. The X-ray diffraction analysis of the glaze A coating of lithium aluminosilicate composition revealed the presence of low expansion phases spodumene ($Li_2O{\bullet}Al_2O_3{\bullet}4SiO_2$) and eucryptite ($Li_2O{\bullet}Al_2O_3{\bullet}2SiO_2$). Spodumene was the major phase that crystallized after firing the glaze coated Si_3N_4 specimens. Eucryptite and Zircon ($ZrSiO_4$) were the other compounds that crystallized out as minor phases. The presence of sharp peaks in the X-ray diffraction pattern indicated that all the compounds were well crystallized. Spodumene and eucryptite phases invert to their β-forms at around 900°C. Because the glaze A coated specimens were fired up to a maximum temperature of 1130°C, the spodumene and the eucryptite phases that crystallized were actually β-spodumene and β-eucryptite, respectively. Thus, a low expansion glaze coating was developed on the Si_3N_4 substrate surface which consisted of basically two portions - the portion which crystallized or devitrified to yield the necessary low expansion phases, and the continuous vitreous matrix that contained the low expansion phases.

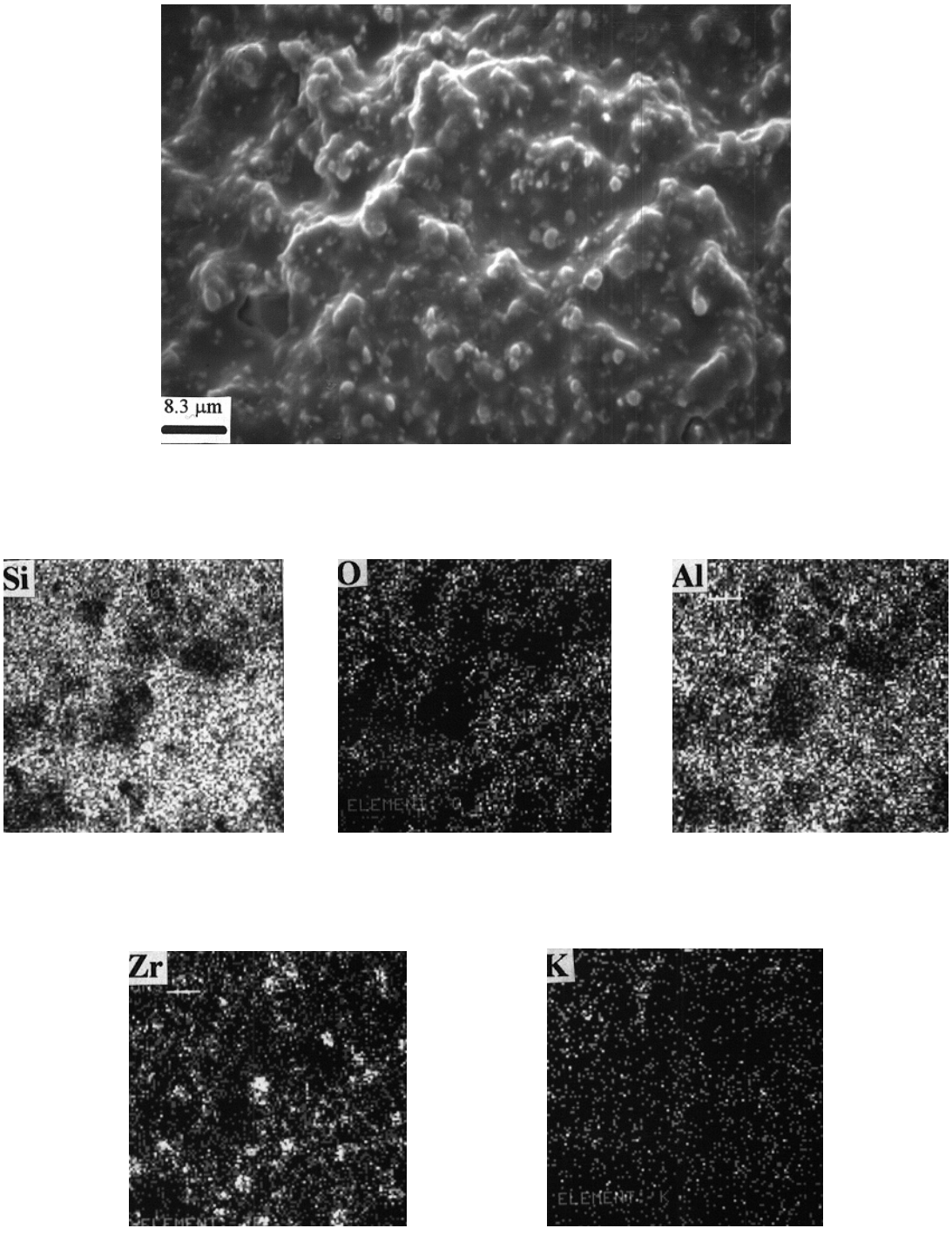

Figure 4.2 SEM micrograph and elemental mappings of glaze A coated Si_3N_4

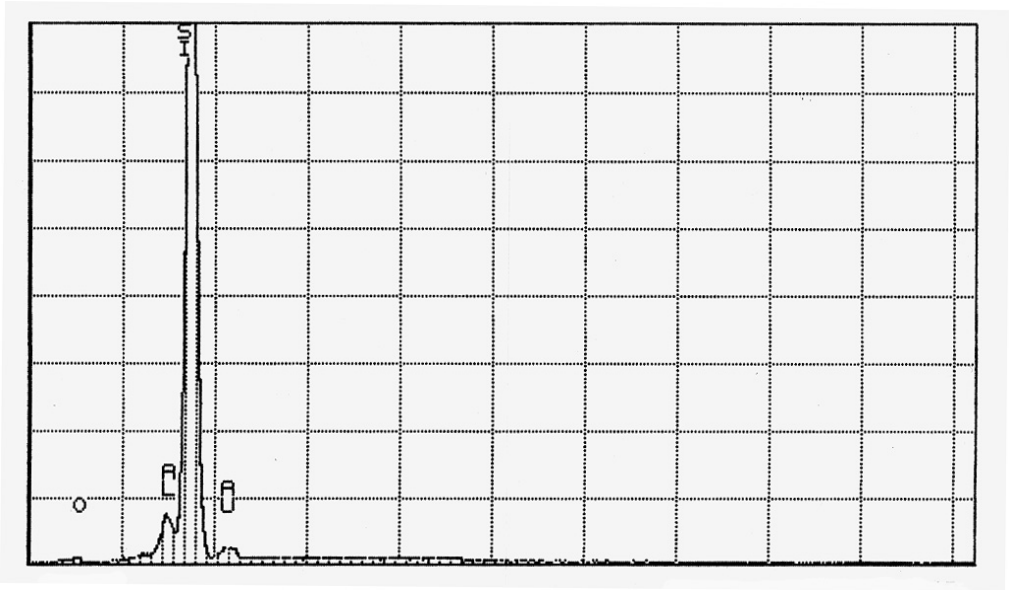

Figure 4.3 EDX spectrum of uncoated Si_3N_4

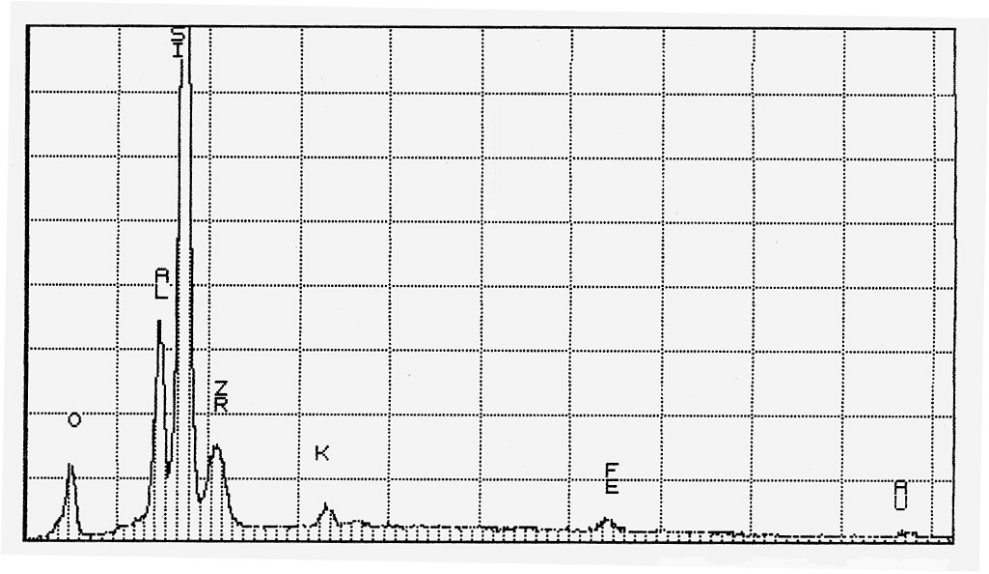

Figure 4.4 EDX spectrum of glaze A coated Si_3N_4

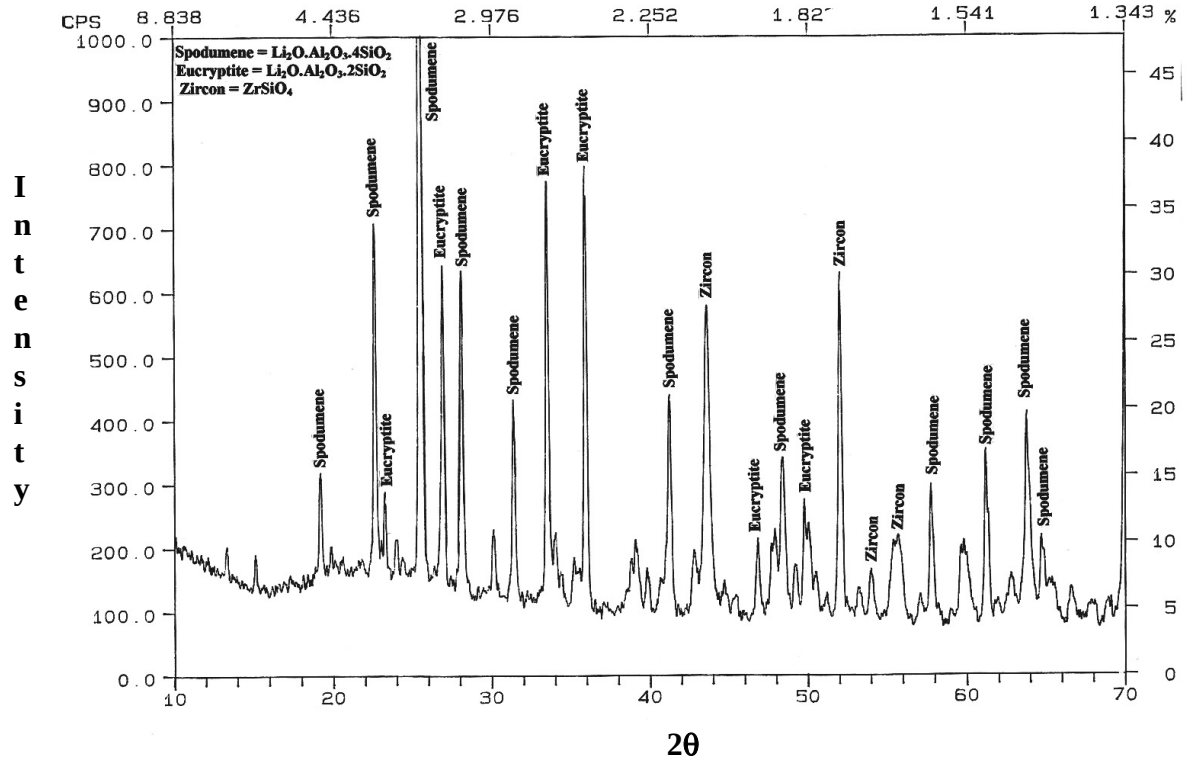

Figure 4.5 XRD pattern of glaze A coated Si_3N_4

4.2.2 Glaze A + Na_2SiO_3 coating

The glaze A coated Si_3N_4 specimens did not develop a very smooth surface as shown in Figure 4.2. To achieve greater surface smoothness, the glaze A coated specimens were fired at different heating schedules with different maximum firing temperatures. After several experimental runs, the optimum firing schedule was found to be the one that had to go to a maximum temperature of 1130°C. Figure 4.6 shows the glaze A coating microstructure developed when fired at a maximum temperature of 1050°C. The SEM micrograph clearly indicates that the coating did not flow very well to cover the substrate surface uniformly. On the other hand, when the glaze A coated specimens were fired above 1130°C, the glazed surfaces developed defects like blisters (2-6mm size bubbles) and pinholes (< 2mm size bubbles) formed

due to overfiring of the glaze. Application of a layer of Na_2SiO_3 solution on the already fired glaze A coated specimens (as mentioned in section 3.3.1) imparted a smooth, glossy surface texture. As shown in the SEM micrograph (Figure 4.7) the surface, in spite of being smooth, developed fine cracks and bubbles. The development of fine cracks is a common glaze defect indicative of poor glaze fit. The addition of Na_2SiO_3 layer on top of the glaze A coated surface and its subsequent firing resulted in a major change in the composition of the original glaze. The increase of Na_2O in the glaze led to an increase in the coefficient of thermal expansion of the glaze, which in turn, led to formation of cracks. The EDX elemental mappings of the area corresponding to the SEM micrograph and the corresponding EDX spectrum (Figure 4.8) reveal the presence of Si, O, Al, and Na.

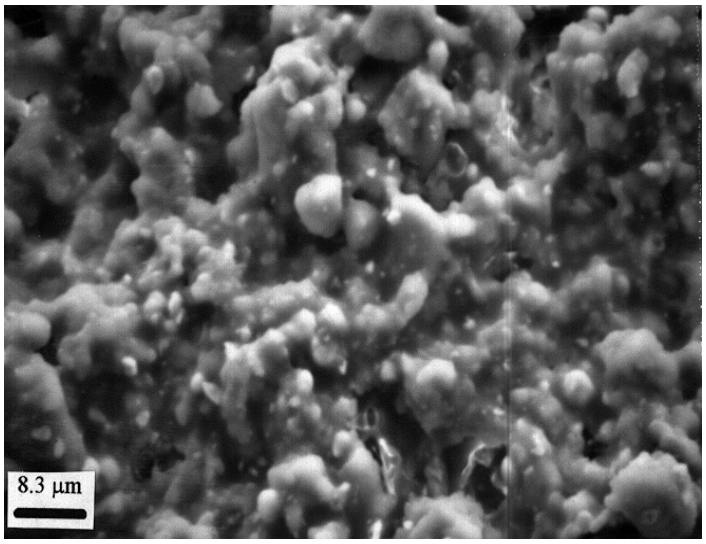

Figure 4.6 SEM micrograph of glaze A coated Si_3N_4 fired at 1050°C

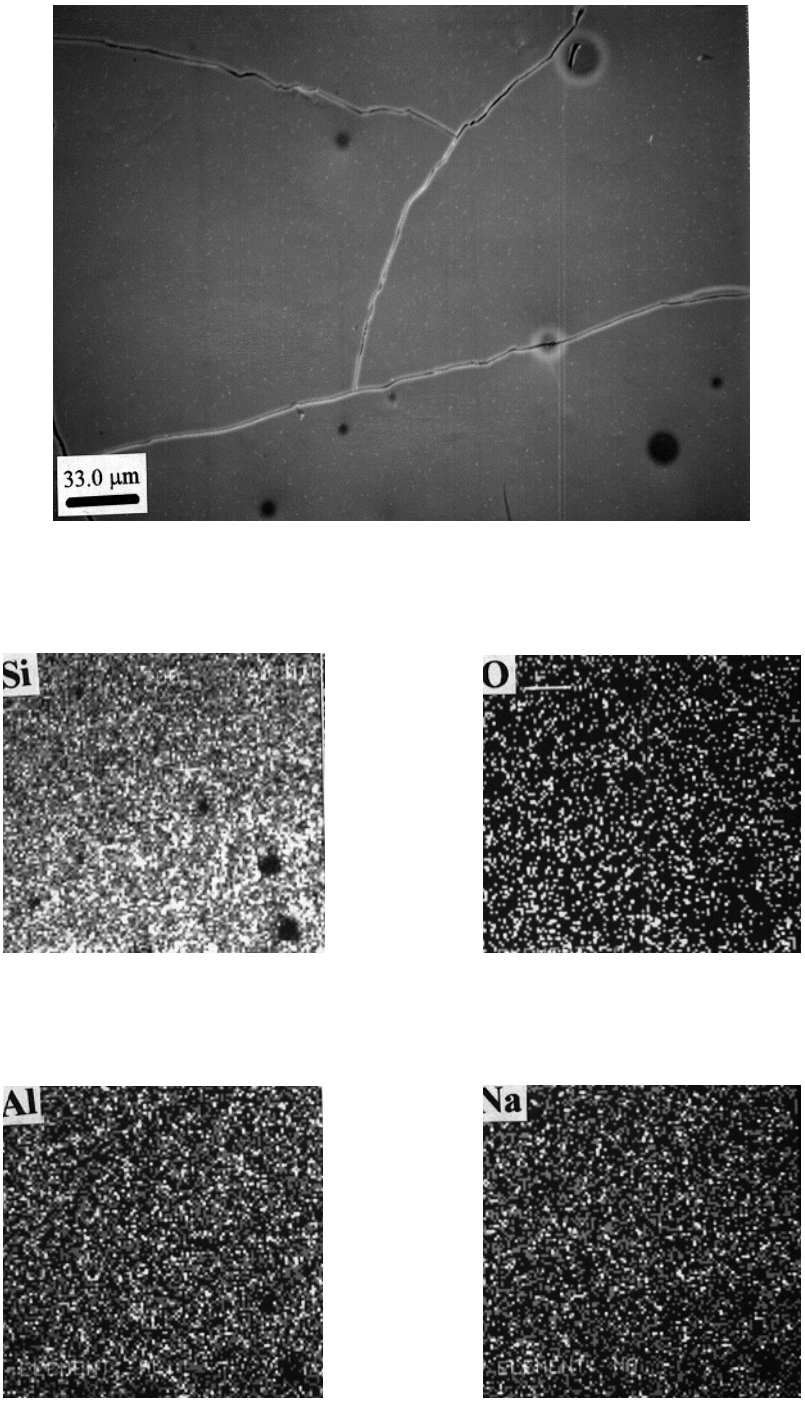

Figure 4.7 SEM micrograph and elemental mappings for glaze A+Na_2SiO_3 coated Si_3N_4

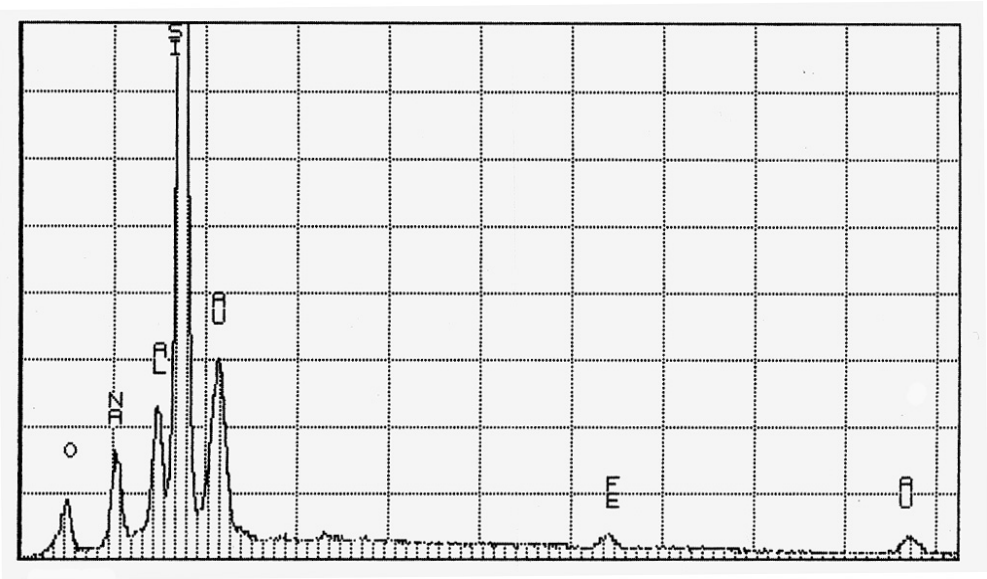

Figure 4.8 EDX spectrum of glaze A+Na_2SiO_3 coated Si_3N_4

4.2.3 Glaze B coating

The glaze of composition B, after being applied on the as processed Si_3N_4 substrate and fired, formed a homogeneous, crack-free and clear coating with a smooth and glossy appearance. The smoothness and the good adherence of the coating depended on the viscosity of the glaze slip. The optimum viscosity of the glaze slip was maintained between 200-300 cP, which resulted in a good coverage of the substrate with the coating. The SEM micrograph, as shown in Figure 4.9, features needle-like particles embedded in a continuous glassy matrix. The corresponding EDX elemental mappings revealed a higher concentration of yttrium on the needle-like particles compared to the surrounding matrix. These needle-like particles were observed by other investigators using a silicon nitride grade containing yttria as sintering agent.[43,44] After conducting X-ray diffraction analysis, the composition of the needle-like particles of size 8 to 12μm were identified as yttrium silicate, Y_2SiO_5. The formation of such needle-like particles of

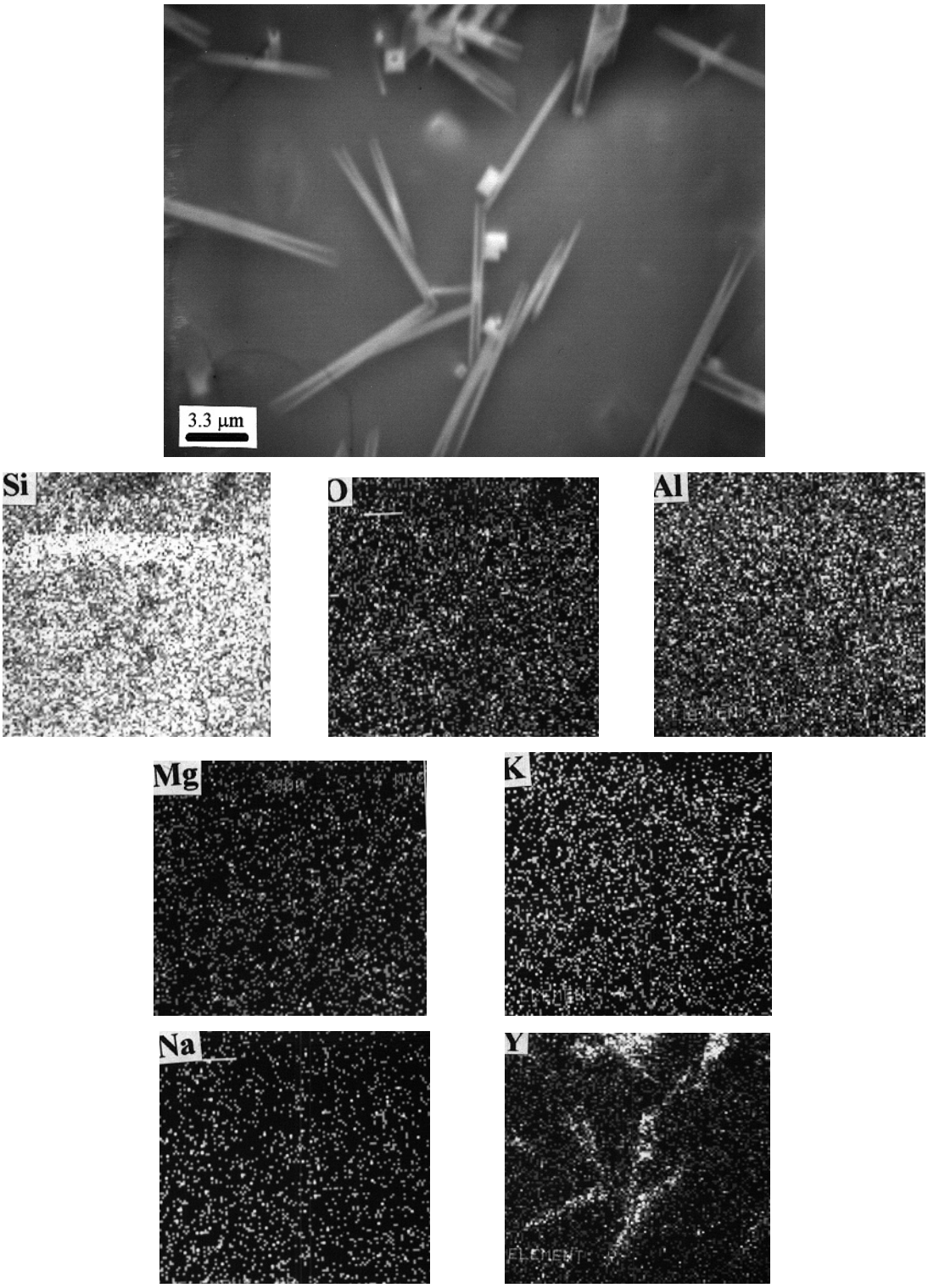

Figure 4.9 SEM micrograph and elemental mappings of glaze B coated Si_3N_4

Y_2SiO_5 was the result of the oxidation of yttria diffusing from the grain boundaries to the surface. This diffusion of yttria occurred in order to equilibrate the chemical composition of the glassy phase. The formation of needle-shaped Y_2SiO_5 only in the case of glaze B coated Si_3N_4 specimen is not fully explained. Apart from the presence of Y, EDX analyses also exhibited almost uniform distribution of the elements Si, O, Al, Mg, K and Na. The EDX spectrum (Figure 4.10) of the entire glaze B coated Si_3N_4 surface also indicated the presence of Si, O, Y, Al, Mg, K and Na. The presence of Mg, K and Na indicate that the glaze of composition B had been successfully

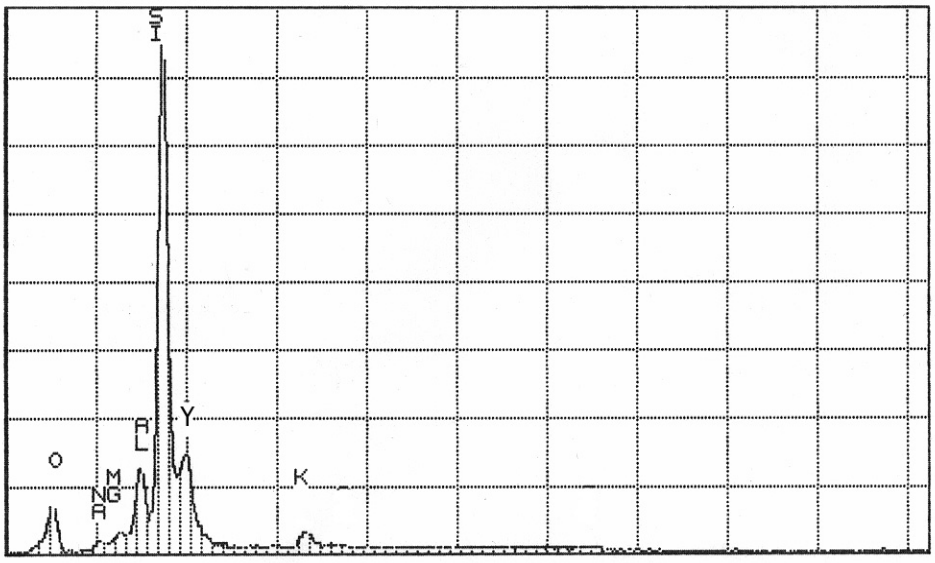

Figure 4.10 EDX spectrum of glaze B coated Si_3N_4

formed on the as fired Si_3N_4 surface. Finally, the X-ray diffraction analysis of the glaze B coating of magnesium aluminosilicate composition established the presence of low expansion cordierite ($2MgO.2Al_2O_3.5SiO_2$) as the major crystalline phase. Figure 4.11 shows the X-ray diffraction pattern of the glaze B coated specimen. The other crystalline phases which were present in minor amounts included corundum (Al_2O_3) and spinel ($MgAl_2O_4$). The sharp peaks, as seen in the X-ray diffraction pattern, are indicative of the fact that all compounds were well crystallized. Because

the glaze B coated specimens were fired to a maximum temperature of 1330°C, the cordierite phases that crystallized were actually α-cordierite - the high temperature α-form of cordierite which forms at temperatures between 1050 and 1460°C.

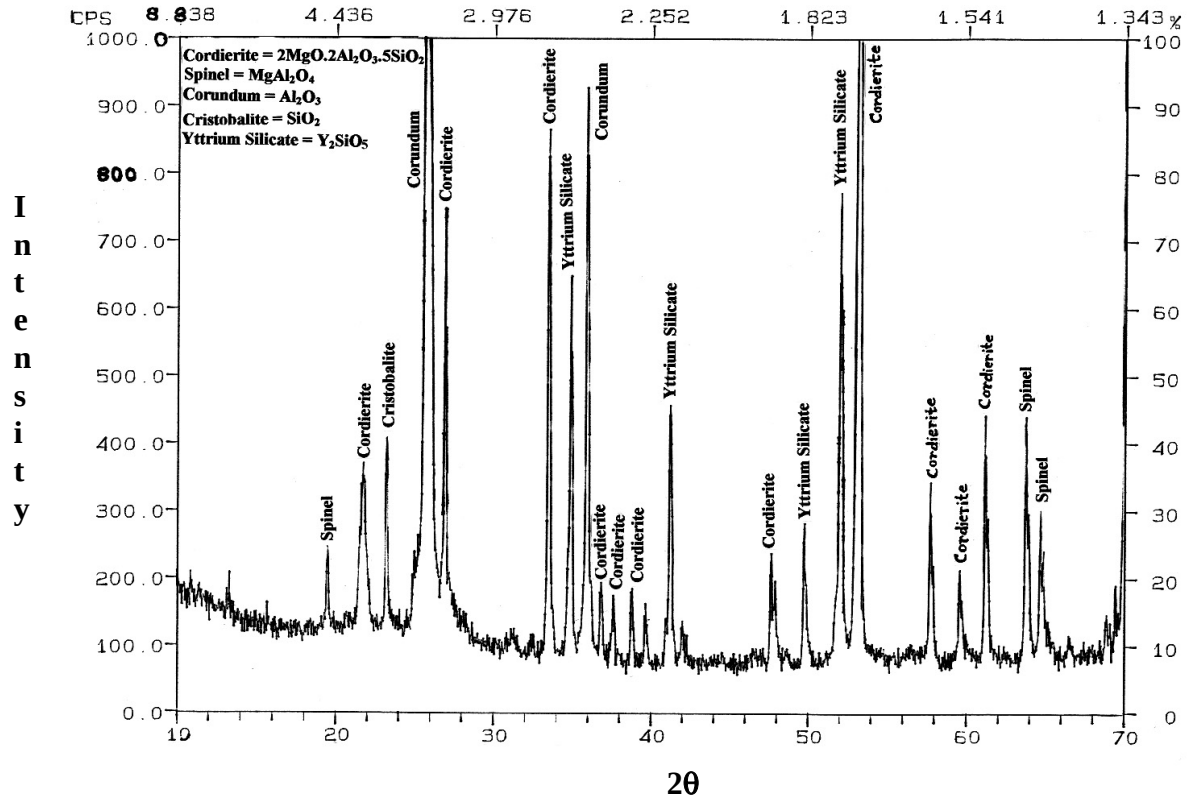

Figure 4.11 XRD pattern of glaze B coated Si_3N_4

4.3 Calculation of coefficients of thermal expansion for glaze A and B

It is known that each oxide present in a glaze exerts its own influence on that glaze, with regard to thermal expansion. Estimated values of coefficients of thermal expansion of glaze A and B compositions can be calculated using the method followed by various investigators.[45,46] To calculate α (coefficient of thermal expansion/CTE) a simple additivity equation (Eq.4.1), proposed by Winkelmann and Schott[22], was used:

$$\alpha = \alpha_1 x_1 + \alpha_2 x_2 + \ldots + \alpha_n x_n = \Sigma \alpha_i x_i \times 10^{-7}\ ^\circ C^{-1} \qquad \text{(Eq.4.1)}$$

where α_i = partial coefficients for various oxides in the glaze composition, and x_i = concentrations of various oxides in the glaze composition taken in cation %. The values of the partial coefficients (α_i) (given by Takahashi[45]) used in the calculation and cation % (x_i) of various oxides present in glaze A and glaze B are given in Table 4.1. Because the partial coefficient value of B_2O_3 was not given by Takahashi and its cation % is relatively low for both glaze A and glaze B, its effect on the overall coefficients of thermal expansion has been neglected. In addition, because these computations were based upon glaze compositions and the compositions of the matured glazes might be different from those calculated due to volatilization and chemical reaction with the body surfaces upon which they are applied, limitations in the use of this method for calculating coefficients of thermal expansion of glazes must be recognized. Also, for the specimen which had a layer of Na_2SiO_3 applied on top of the matured glaze A coating, the coefficient of thermal expansion would be significantly different than that of the matured glaze A coated specimen. Thus, although any such calculated coefficients of thermal expansion cannot be very accurate because of the number of unwarranted assumptions involved, such calculations allow estimation of the expected values. Using the above additivity equation, the CTE of glaze A and B were calculated to be 2.7 x 10^{-6} $^\circ C^{-1}$ and 1.4 x 10^{-6} $^\circ C^{-1}$, respectively, both of which are lower than that of the Si_3N_4 substrate. The CTE of hot-pressed Si_3N_4 is generally known to be 3.2 x 10^{-6} $^\circ C^{-1}$.[40]

Oxide	**Coefficient, α_i (by Takahashi)**	**Cation %, x_i Glaze A**	**Cation %, x_i Glaze B**
SiO_2	0.05	50.76	70.60
ZrO_2	-1.43	15.40	0.61
Al_2O_3	0.27	13.51	16.19
MgO	0.33	--	8.87
Li_2O	2.00	15.30	--
Na_2O	2.69	--	0.90
K_2O	3.00	4.06	0.35
CaO	1.30	--	0.61
Fe_2O_3	0.32	--	0.43
B_2O_3	--	0.98	1.41

Table 4.1 Chart used for calculation of coefficients of thermal expansion

4.4 Room temperature flexural strength evaluation

The room temperature flexural strengths of uncoated and coated as fired Si_3N_4 specimens obtained by conducting four-point bending tests are shown in Figure 4.12. The flexural strength or the bend strength of a specimen is the maximum tensile stress at failure, often referred to as the modulus of rupture, or MOR. The flexural strengths of the specimens were calculated using the general flexural stress formula[8]:

$$S = \frac{3PL}{4bd^2} \qquad \text{(Eq.4.2)}$$

where P = breakload; L = support span; b = specimen width; d = specimen thickness

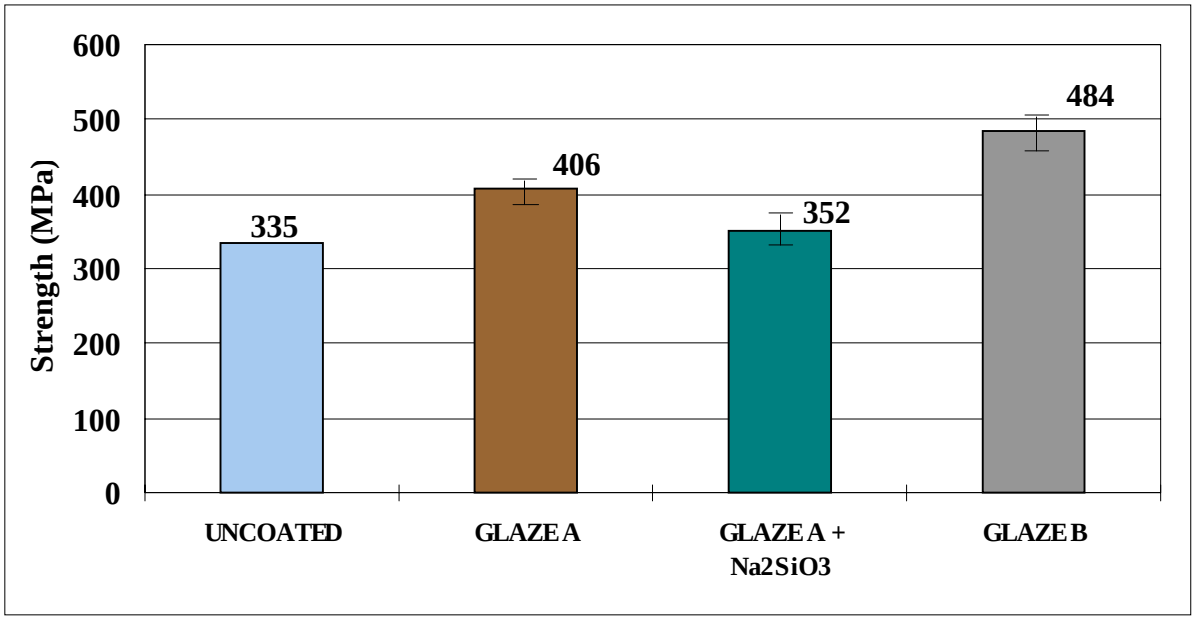

Figure 4.12 Four-point bending flexural strengths of uncoated and coated Si_3N_4

The flexural strength of uncoated as fired Si_3N_4 was reported to range between 320-350 MPa.[47] As indicated in Figure 4.12, the coated specimens showed increased flexural strength as compared to uncoated Si_3N_4. A comparison of the coated specimens with the uncoated as fired

Si_3N_4 taken as reference, showed the least strength improvement for glaze A+Na_2SiO_3 coating (+ 5.1% of initial strength). Specimens with glaze A coating also showed an increase in flexural strength (+ 21.2% of initial strength), while for glaze B coating an appreciable strength increment (+ 44.5% of initial strength) was observed. Because the CTE of glaze A and glaze B were calculated to be lower than that of Si_3N_4 substrate, strength improvements due to the coatings were expected and were corroborated by the flexural strength test results.

The ranges of the mean flexural strength values for the three sets of coated specimens were calculated for 95% confidence intervals as presented in Table 4.2.

	Glaze A	**Glaze A+Na_2SiO_3**	**Glaze B**
Strength (MPa)	406 ± 21	352 ± 22	484 ± 24

Table 4.2 Range of mean flexural strengths calculated with Student's t-test

In order to illustrate the effects of the coatings on the strength distributions of the three sets of specimens, strength data were plotted as Weibull plots. The data for each of the five specimens corresponding to each coating were combined to give one curve. The Weibull plots were generated from the well known form of the Weibull equation of failure probability[8]:

$$F = 1 - \exp\left[- V_E \left(\left(\sigma_f - \sigma_u \right) / \sigma_o \right)^m \right] \qquad \text{(Eq.4.3)}$$

where F is the estimated probability of failure of a specimen, V_E is the effective sample volume under stress (depends on the sample size and loading configuration), σ_f is the fracture strength, σ_u is the threshold stress (stress below which the probability of failure equals zero), σ_o is a constant known as the scale parameter (often selected as the characteristic stress, at which the probability of failure is 0.632), and m is the Weibull modulus. Threshold stress, σ_u is often conservatively set

equal to zero, yielding the two parameter Weibull equation where the effective volume for four-point bending is taken to be $V(m+2)/4(m+1)^2$. Thus, Eq.4.3 can be written as

$$F = 1 - \exp\left[- V(m+2)/4(m+1)^2 \left(\sigma_f / \sigma_o \right)^m \right] \qquad \text{(Eq.4.4)}$$

Rearranging the above equation and taking the natural logarithm twice gives:

$$\ln \ln\left[1/(1-F) \right] = K + m \ln \sigma_f \qquad \text{(Eq.4.5)}$$

where constant $K = \ln \left[V(m+2)/4(m+1)^2 \right] - m \ln \sigma_o$

Using Eq.4.5, the Weibull modulus, m, was obtained from the slope of the curve by plotting ln ln (1/(1-F)) against ln σ_f. Table 4.3 shows the organization of experimental data to plot Weibull curves where F is calculated as n/(N+1), n being the ranking of the sample and N the total number of samples.

Number of ordered data	Measured Strength σ (MPa) GlazeA	Measured Strength σ (MPa) GlazeA+Na_2SiO_3	Measured Strength σ (MPa) GlazeB	Estimated probability of failure F ≈ n/(N-1)
1	390	340	462	0.167
2	392	341	466	0.333
3	403	343	491	0.500
4	416	352	494	0.667
5	430	383	507	0.833

Table 4.3 Organization of experimental data to plot Weibull curve

The Weibull plot, as shown in Figure 4.13 reveals that the distributions of the glaze A and glaze A+Na_2SiO_3 coated specimens are very close to one another. The plot also suggests that the glaze B coated specimens exhibit a higher Weibull modulus. The Weibull modulus, m, is a measure of the scatter in strength of a material. A high value of m would indicate low scatter.

The m values, calculated from the slope of each curve, corresponding to glaze A, glaze A+Na_2SiO_3 and glaze B are 12.3, 10.7, and 19.4, respectively. Thus, glaze B coated specimens, showing higher m value than the other two sets of specimens, may indicate higher reliability.

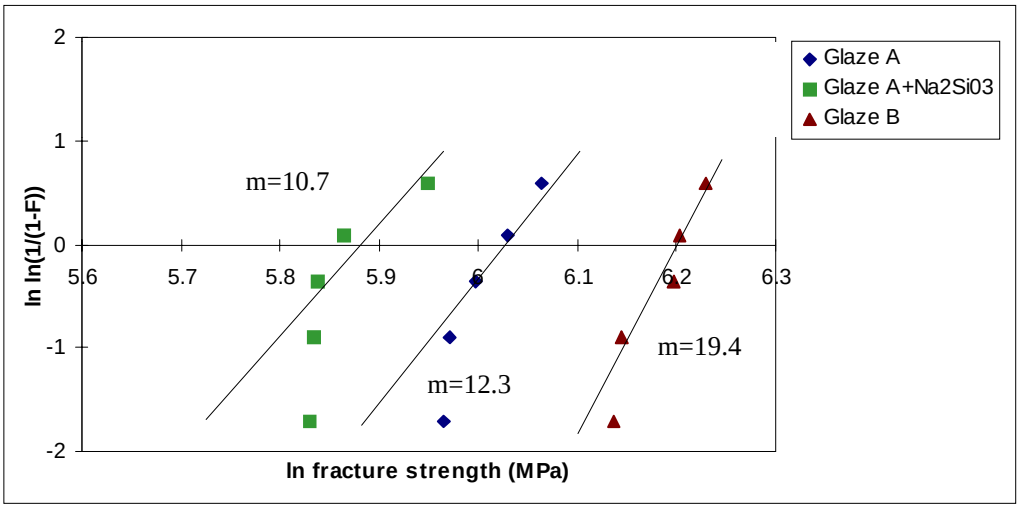

Figure 4.13 Weibull curve for strength data of coated Si_3N_4

4.5 Study of fracture surfaces of uncoated and coated Si3N4

Following strength testing, scanning electron microscopy (SEM) was employed to examine the fracture surfaces of the broken specimens. Figure 4.14(a) shows the SEM micrograph of the fracture surface of a Si_3N_4 specimen with the uncoated as fired surface. In the micrograph, the arrows indicate the origin of failure located at the edge of the uncoated as fired surface. Figure 4.14(b) illustrates the same fracture surface at a higher magnification of 1000x where a large pore or void, located at the edge of the specimen, can be easily identified. Similar smaller size voids are also present near the edge of the specimen. These kind of surface flaws are generally the consequence of material processing and can be preferential failure origins.

(a)

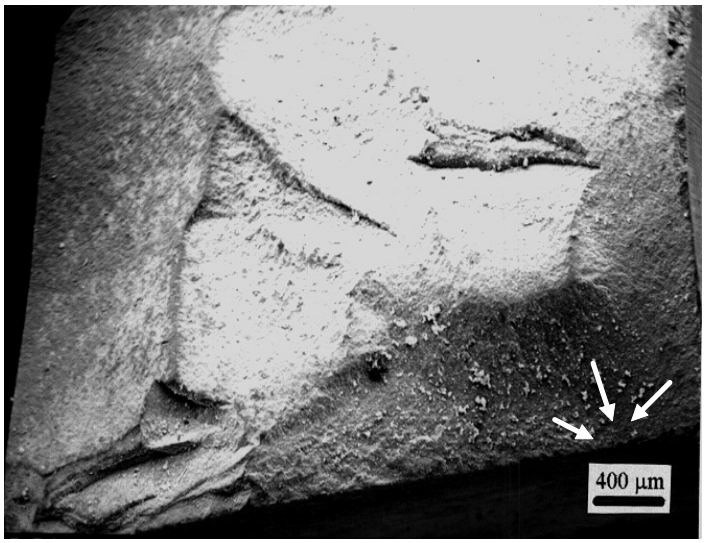

(b)

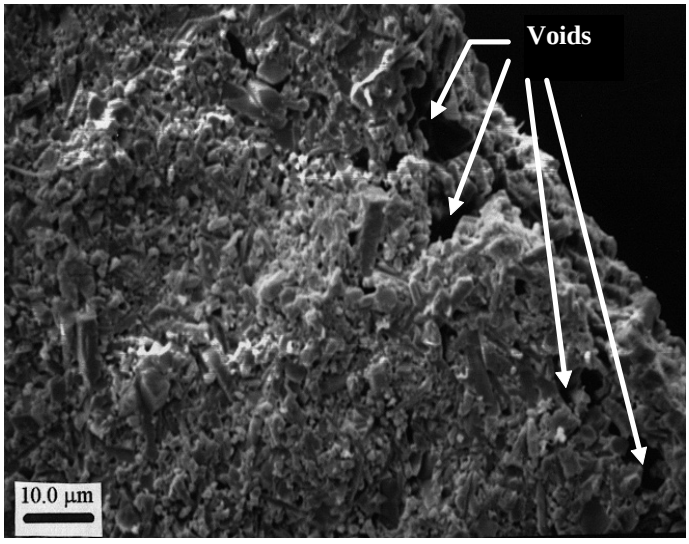

Figure 4.14 SEM micrograph of the fracture surface of uncoated as fired Si_3N_4 at (a) low and (b) high magnification

The SEM micrograph of the fracture surface of Si_3N_4 specimen is shown in Figure 4.15 where the glaze A coated surface was broken in tension under four-point flexure. The arrows

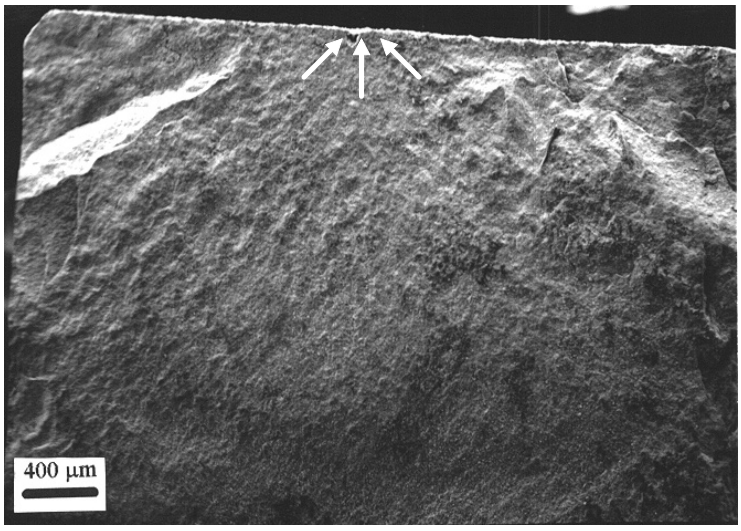

Figure 4.15 SEM micrograph of the fracture surface of glaze A coated Si_3N_4 at low magnification

indicate the approximate region where the failure was initiated. It was noted that the failure originated at the edge of the glaze A coated surface. The SEM micrograph (Figure 4.16) of the same fracture surface at a higher magnification of 1800x illustrates the coating/substrate interface. As observed from the corresponding EDX elemental mappings, the coating thickness varied between 5 and 12μm. The SEM micrograph and the corresponding EDX analyses indicate that the voids or pits that were present on Si_3N_4 surface at the coating/substrate interface were filled with the coating material. In addition there appeared relatively good mechanical bonding at the interface. The strength increment of the glaze A coated specimens can thus be attributed to the development of compressive stress at the as fired Si_3N_4 surface due to the presence of the low expansion glaze on its surface. The development of surface compressive stress, opposing the applied tensile stress, led to the net reduction of the applied tensile stress. Filling in of the surface

flaws by the coating, responsible for the reduction of the length of the surface flaws, was another factor which led to strength improvement of the glaze A coated specimens. However, the cross-sectional view of the coating clearly shows that the coating did not develop an even and smooth surface and, hence, did not entirely fill up the pits/voids present in the Si_3N_4 surface. Thus, the glaze A coating was able to enhance the room temperature flexural strength of the as fired Si_3N_4, but not as much as the glaze B coating. Also, because the calculated CTE of glaze A (2.7×10^{-6} $°C^{-1}$) was found to be higher than that of glaze B (1.4×10^{-6} $°C^{-1}$), the compressive stress created at the glaze A coated Si_3N_4 surface would be lower than that for glaze B and, hence, the glaze A coated Si_3N_4 should exhibit a lower flexural strength.

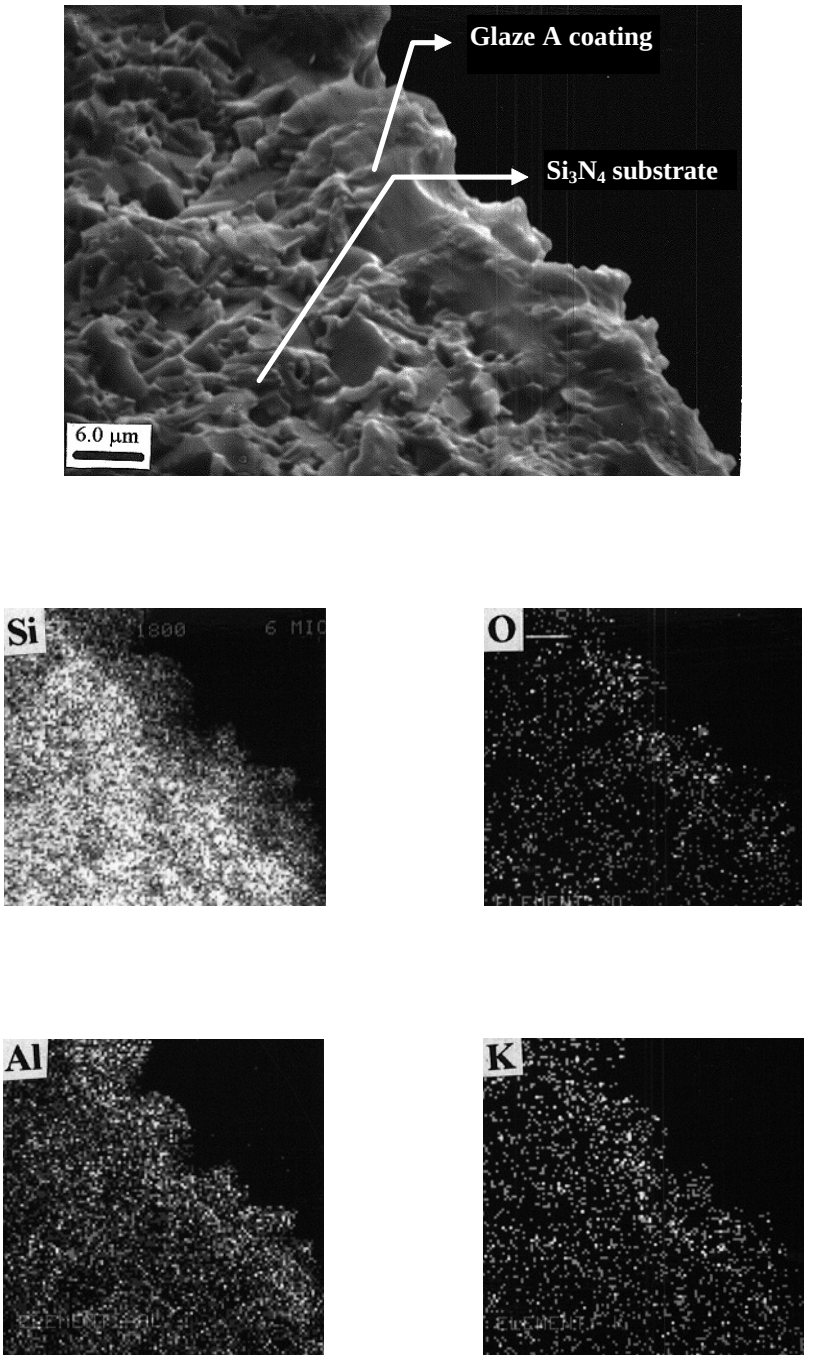

Figure 4.16 SEM micrograph and corresponding EDX elemental mappings of the fracture surface of glaze A coated Si_3N_4 at high magnification

The SEM micrograph, as shown in Figure 4.17, exhibits the fracture surface of the Si_3N_4 specimen with the glaze $A+Na_2SiO_3$ coating broken in tension under four-point bending. The arrows in the figure indicate the location of the failure origin. Observations of the fracture surfaces of glaze $A+Na_2SiO_3$ coated specimens revealed that the thickness of the coating decreased along the edges of the specimen (shown in Figure 4.17). It was found that the location of the failure origin was at the edge of the specimen where the coating was almost absent, instead of being at the coating / matrix interface. This was possibly due to the reason that the coating, being so soft, had chipped off from the specimen edge under the flexural stress. The SEM micrograph of Figure 4.18 shows a closer view of the same fracture surface where the coating/matrix interface and also the bubbles formed in the coating can be easily identified. This

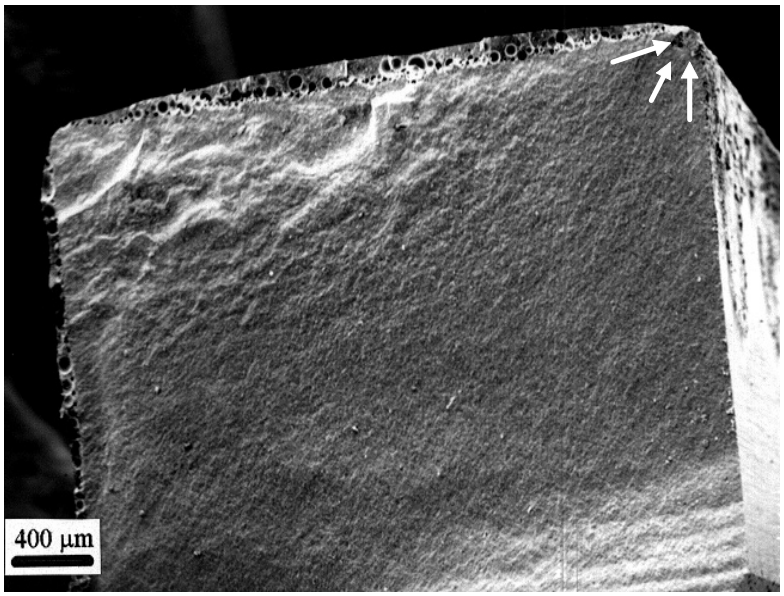

Figure 4.17 SEM micrograph of the fracture surface of glaze $A+Na_2SiO_3$ coated Si_3N_4 at low magnification

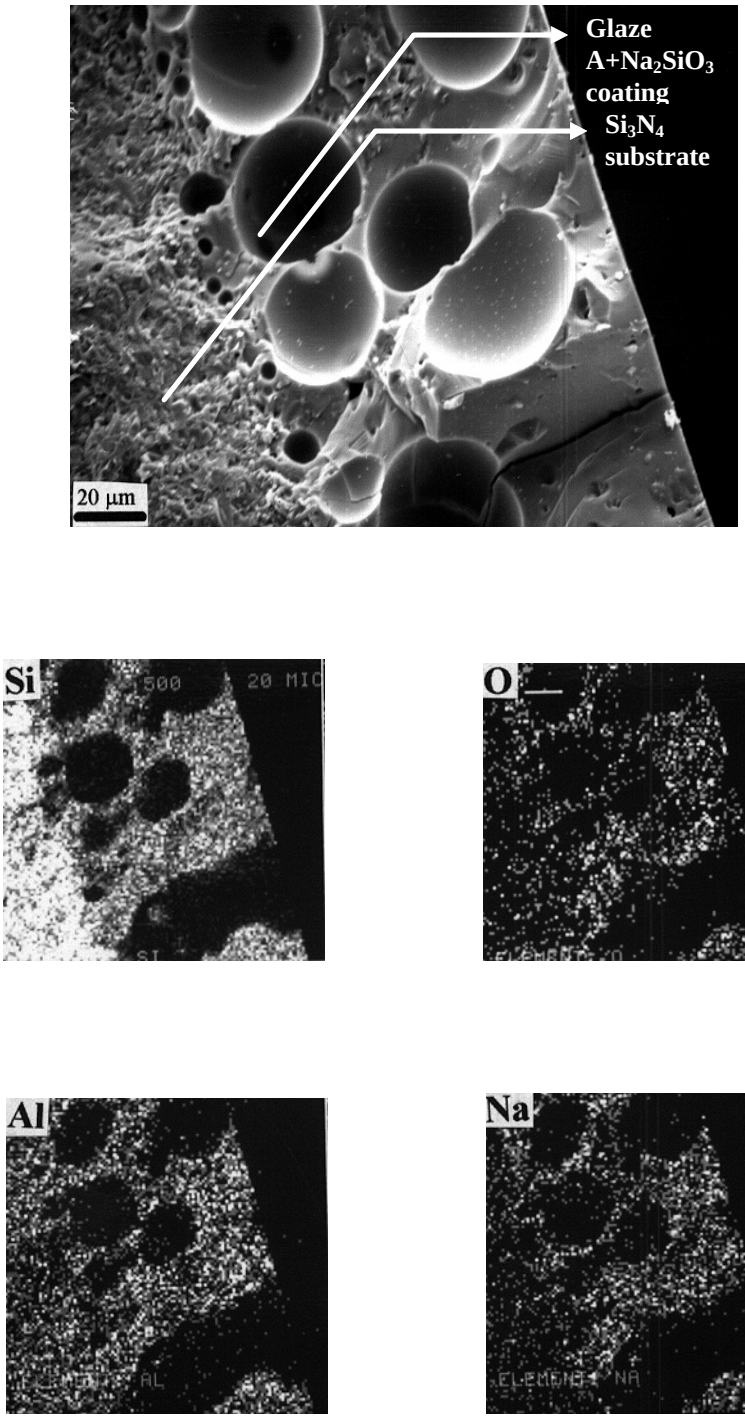

Figure 4.18 SEM micrograph and corresponding EDX elemental mappings of the fracture surface of glaze A+Na_2SiO_3 coated Si_3N_4 at high magnification

micrograph exhibits totally different characteristics when compared to Figure 4.16. When a layer of Na_2SiO_3 was applied on to the matured glaze A coating, the characteristics of the original coating changed completely. The sodium silicate layer, when applied on to the glaze A coated Si_3N_4 specimen and then subsequently fired, facilitated the oxidation mechanism of Si_3N_4 which led to the inward diffusion of O_2 and outward diffusion of N_2 gas, according to Eq.4.6:

$$Si_3N_4 + 3O_2 \Leftrightarrow 3SiO_2 + 2N_2 \qquad \text{(Eq.4.6)}$$

This release of gases during the oxidation was responsible for the formation of bubbles as seen in Figure 4.18. The corresponding X-ray maps revealed an even distribution of Si, O Al and Na indicating the formation of a sodium aluminate silicate phase. The X-ray maps also showed that the sodium silicate layer after firing penetrated into the Si_3N_4 substrate up to a depth of about 120μm. The specimens with glaze A+Na_2SiO_3 coating showed a 5.1% strength increment. The sodium silicate formed a glassy coating which was able to flow over the surface irregularities of the matured glaze A coating leading to increased surface smoothness. However, the key factors which inhibited the strength of the glaze A+Na_2SiO_3 coated specimens to increase by any appreciable amount were - (i) the increased percentage of Na_2O on the glazed surface which resulted in an increase in the effective coefficient of thermal expansion of the coating and led to the formation of fine cracks on the surface, and (ii) the presence of bubbles or pores created due to the release of gases.

Figure 4.19 shows the SEM micrograph of the fracture surface of Si_3N_4 specimen with the glaze B coated surface. As shown by arrows in the figure, the region around the failure origin was located at the edge of the glaze B coated surface. Figure 4.20 presents a higher magnification view of the same fracture surface where the glaze coating on the surface can be clearly distinguished from the Si_3N_4 substrate underneath. As observed from the cross-sectional view and the corresponding EDX elemental mappings of Figure 4.20, the coating has a uniform thickness of about 9μm. The EDX analyses also indicate the higher concentration of yttrium at the coating surface which was the result of the oxidation of yttria diffusing from the grain

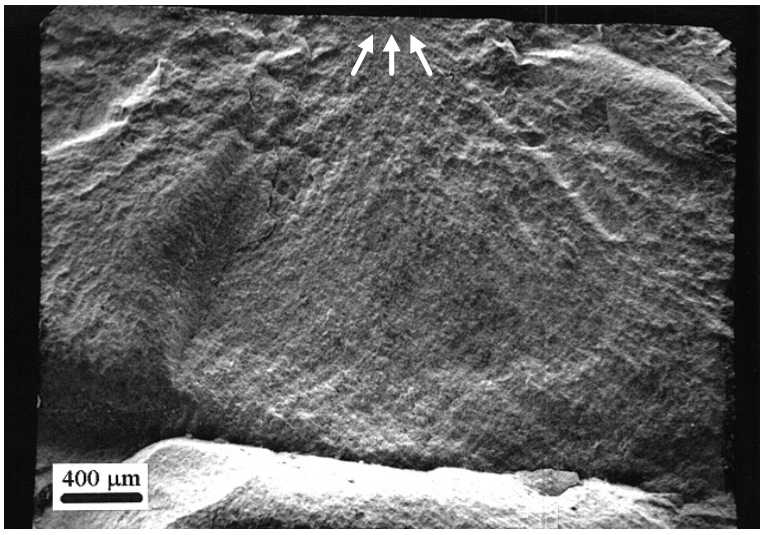

Figure 4.19 SEM micrograph of the fracture surface of glaze B coated Si_3N_4 at low magnification

boundaries to the surface to form the needle-like particles of Y_2SiO_5 as previously shown in Figure 4.9. After comparing between Figures 4.16 and 4.20, which illustrate the cross-sectional views of the coatings A and B, it is clearly evident that the glaze B coating had achieved greater surface smoothness. The coating had flowed well over the substrate surface successfully penetrating into the flaws present on the surface and had achieved good mechanical bonding at the coating/substrate interface. Thus, the glaze B coated as fired Si_3N_4 specimens exhibited a substantial strength enhancement. In addition to all the causes that led to the strength increment for glaze A coating, the glaze B resulted in greater reduction of surface defects and also higher compressive surface stress formation due to lower CTE than glaze A, and hence, resulted in higher strength of the as fired Si_3N_4 specimen.

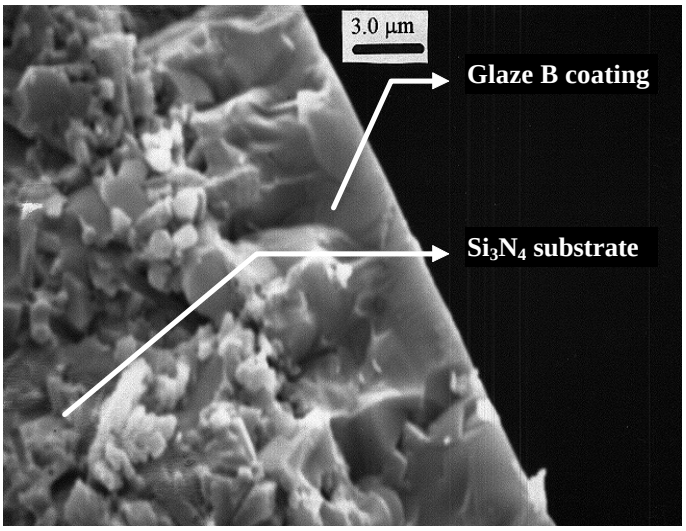

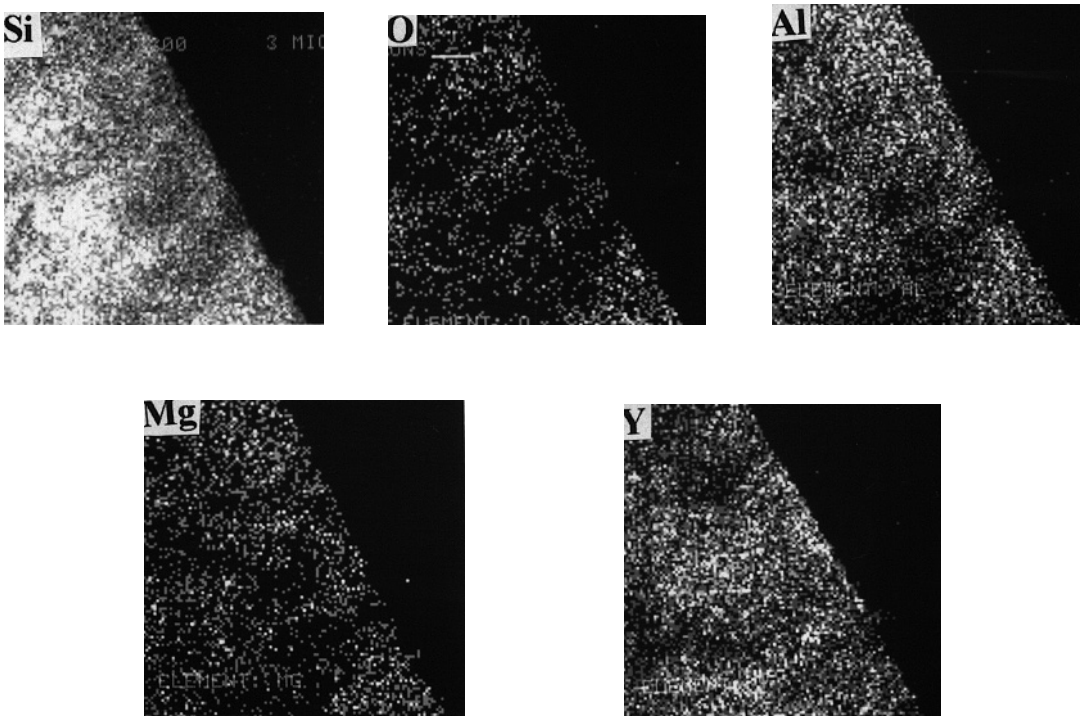

Figure 4.20 SEM micrograph and corresponding EDX elemental mappings of the fracture surface of glaze B coated Si_3N_4 at high magnification

4.6 Wear tests

Figures 4.21-4.24 contain the wear profile diagrams obtained from running the surface profiler over the wear tracks of the uncoated, glaze A coated, glaze A+Na_2SiO_3 coated and glaze B coated Si_3N_4 flat specimens, respectively. A comparative evaluation of all these figures show that the sample coated with glaze A+Na_2SiO_3 was most severely effected by wear. This was evident from the depth of the valley along the wear track shown in Figure 4.23 and also from the wear depth and the wear volume given in Table 4.4. In comparison, the uncoated specimen showed negligible wear (clearly evident from Figure 4.21 where there is no such deep valley as shown in Figures 4.22, 4.23 and 4.24). The areas mentioned in the wear diagrams below represent the cross sectional worn out area along the wear tracks of the Si_3N_4 flat specimens.

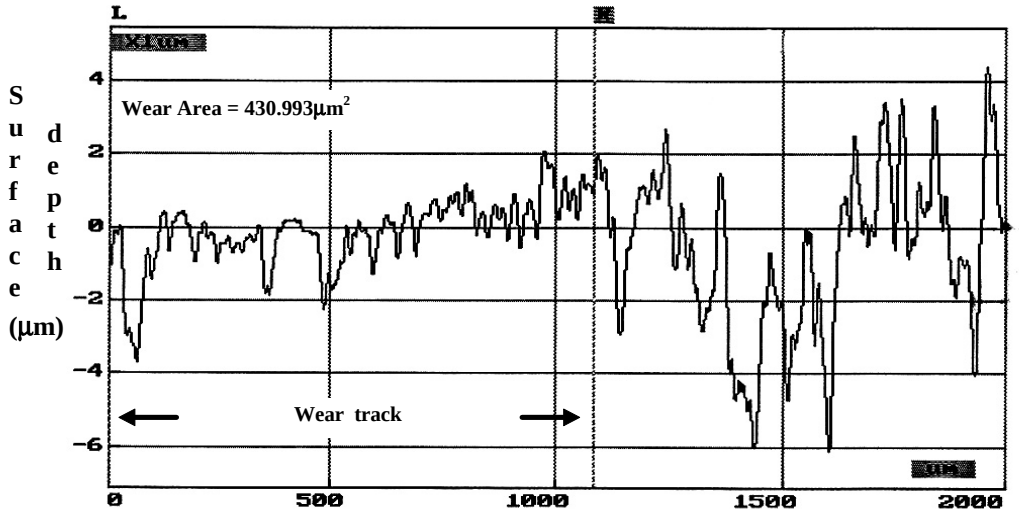

Figure 4.21 Wear profile diagram for uncoated as fired Si_3N_4

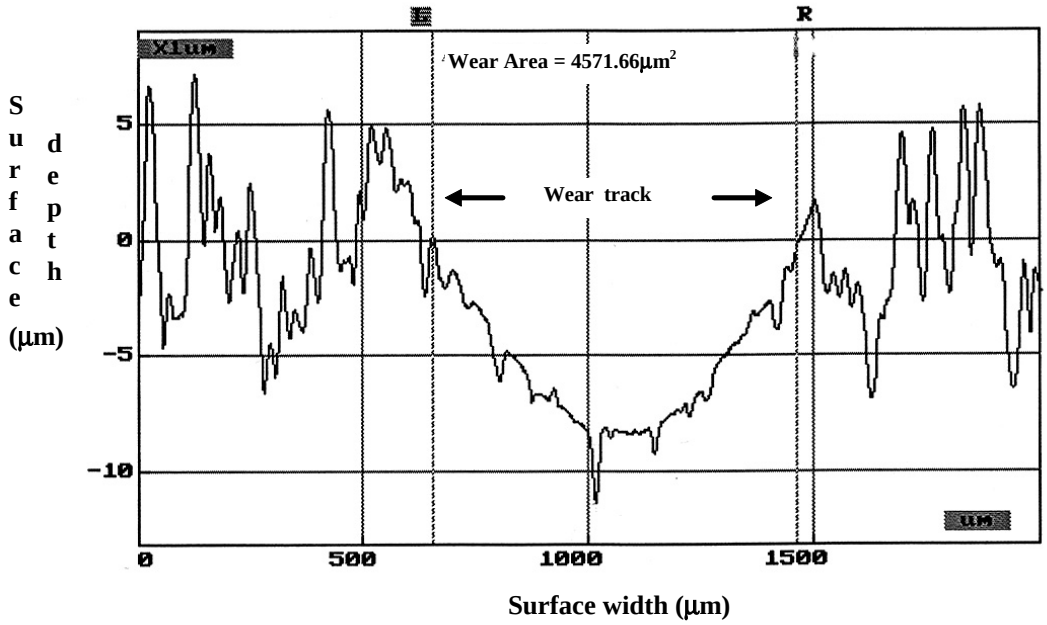

Figure 4.22 Wear profile diagram for glaze A coated Si_3N_4

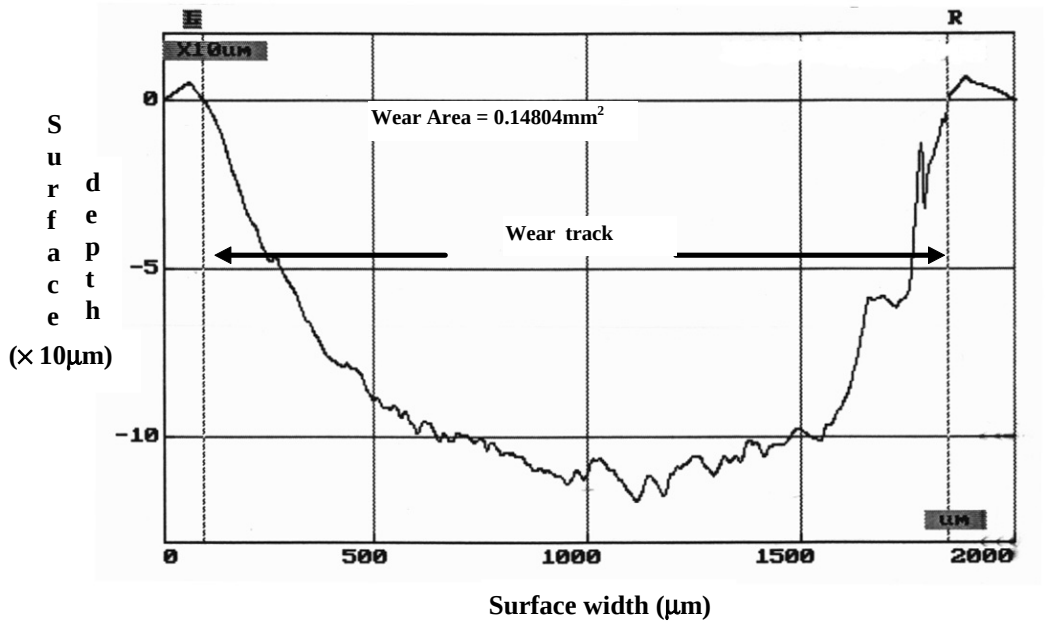

Figure 4.23 Wear profile diagram for glaze A+Na_2SiO_3 coated Si_3N_4

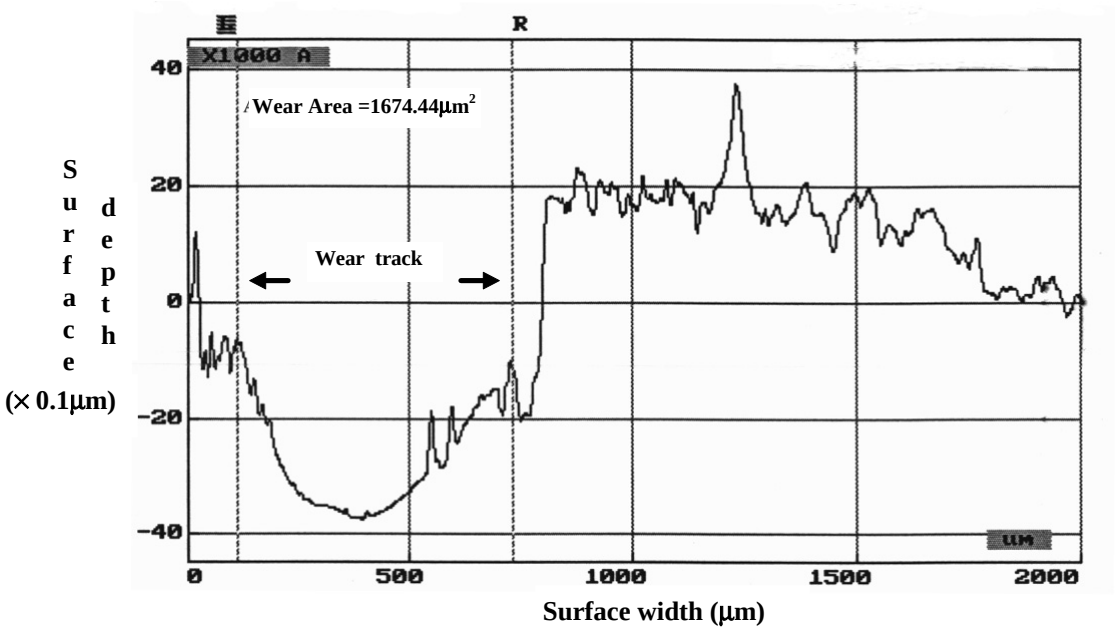

Figure 4.24 Wear profile diagram for glaze B coated Si_3N_4

It was also noted that the wear was greater in case of glaze A coated specimen as compared to glaze B (evident from the wear depth and the wear volume as given in Table 4.4). Details of the amount of wear measured by the surface profiler is given in Table 4.4. The coefficient of friction (μ), given in Table 4.4, was calculated from the frictional force measured for each sample under a normal load of 9.8N. It was noted that the μ value for each sample was not significantly different

	coating thickness (μm)	wear depth (μm)	wear vol = wear area x sliding distance of 6.2 mm	coefficient of friction, (μ)
Uncoated	-	2	.0026	0.845
Glaze A	5-12	8	.0283	0.848
Glaze A+Na_2SiO_3	120	115	.9178	0.866
Glaze B	9	3.6	.0104	0.846

Table 4.4 Wear data as measured by the surface profiler

except for the glaze A+Na_2SiO_3 specimen. This difference in μ was possibly because of the breakup of the glaze leading to surface roughness. Figure 4.25 shows the SEM micrograph of the wear scar on the 52100 steel ball developed after sliding against uncoated as fired Si_3N_4 flat specimen. The steel ball developed a deep groove along its slip region from where material was transferred on to the Si_3N_4 flat specimen. The EDX spectrum of the wear surface of the steel ball given in Figure 4.26 shows very little material transfer from Si_3N_4, as indicated by the small peaks of Si and Al. Figure 4.27 is a micrograph of the wear track on uncoated Si_3N_4 flat. As evident

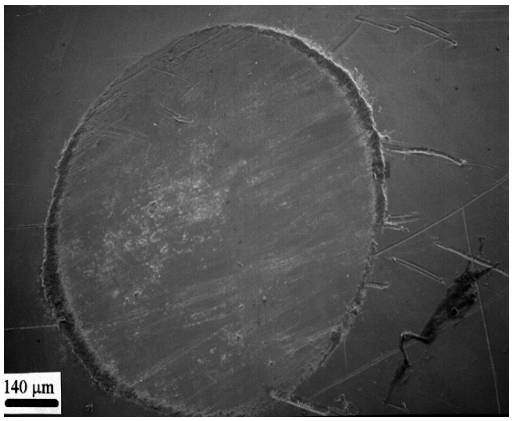

Figure 4.25 SEM micrograph of wear scar on steel ball developed after sliding against uncoated as fired Si_3N_4 flat

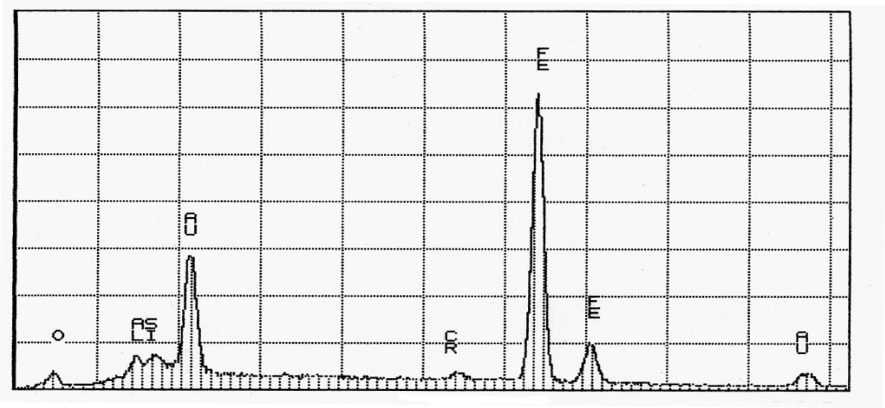

Figure 4.26 EDX spectrum of steel ball after sliding against uncoated Si_3N_4

from the corresponding X-ray maps, a significant amount of metal transferred from the steel ball and the damage of the Si_3N_4 flat was much less than that of the steel ball. The large peak of Fe, shown in the EDX spectrum of the wear track on Si_3N_4 of Figure 4.28, also confirms this fact.

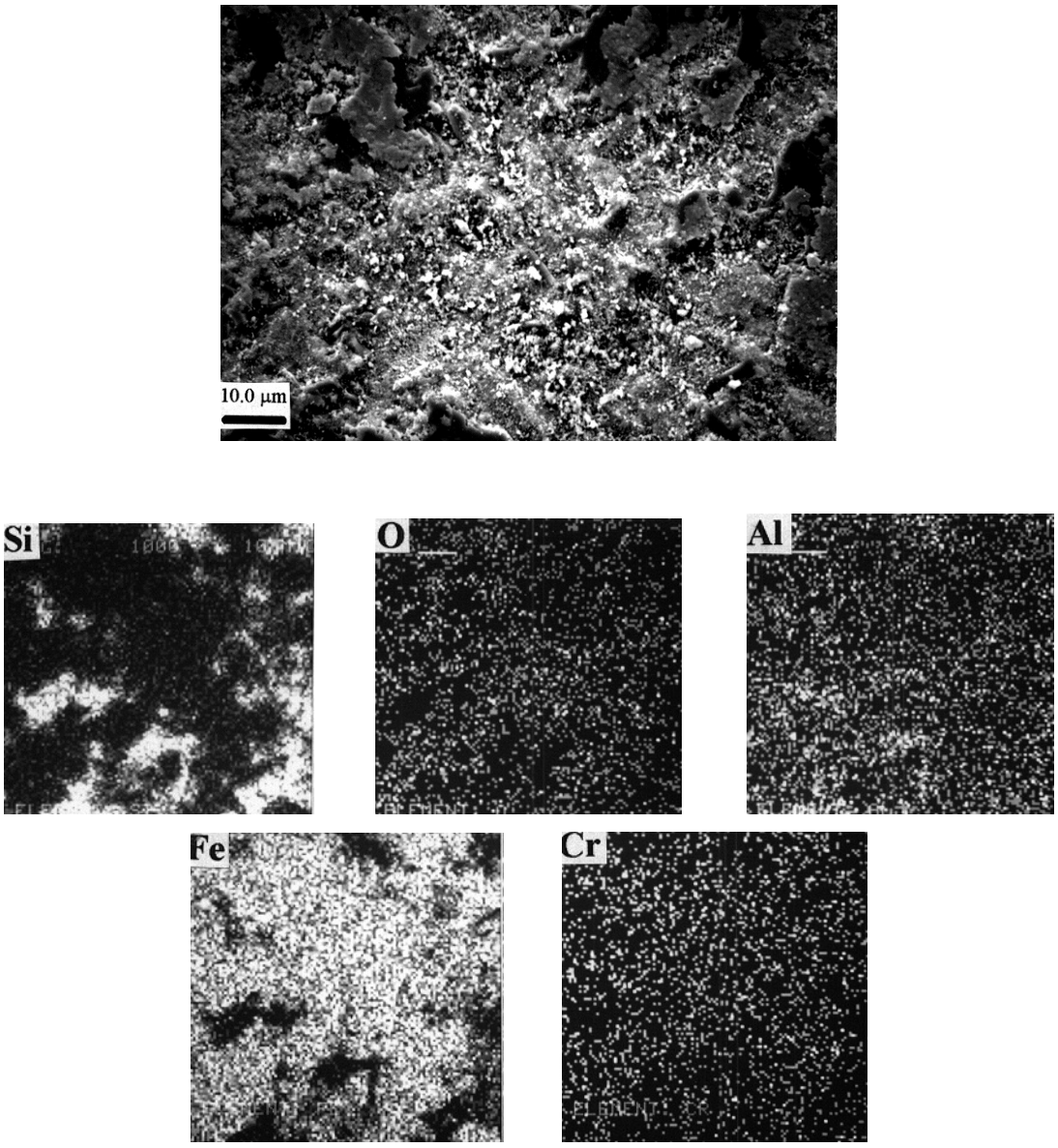

Figure 4.27 SEM micrograph and EDX elemental mappings of wear track on uncoated Si_3N_4 flat.

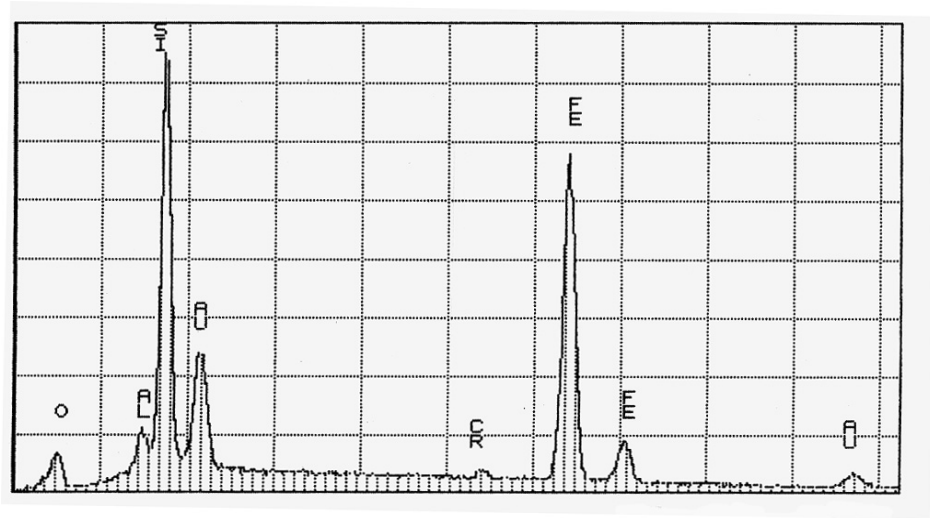

Figure 4.28 EDX spectrum of the wear track on uncoated Si_3N_4 flat

Figure 4.29 shows the micrograph of the wear scar formed on the steel ball developed after sliding against glaze A coated Si_3N_4 flat specimen. The wear on the steel ball sliding against glaze A coated specimen was lower than that for the uncoated specimen as evident from comparing Figures 4.25 and 4.29. Also, material transferred from the coated Si_3N_4 flat on to the steel ball was higher than that for the uncoated one. This is indicated by the EDX spectrum of the steel ball wear surface of Figure 4.30 where the peaks of Si and Al are comparatively much higher. The SEM micrograph and the corresponding EDX analyses of the wear track on the glaze A coated Si_3N_4 flat is shown in Figure 4.31. It reveals that a lesser amount of material was transferred from the steel ball in this case, compared to the steel ball sliding against the uncoated specimen. This is also substantiated by the comparatively smaller peak of Fe, as indicated by the EDX spectrum of the glaze A coated wear surface of Figure 4.32. In this case, materials were transferred mutually between the ball and the flat specimen indicating that the coating made the Si_3N_4 material less wear resistant.

Figure 4.29 SEM micrograph of wear scar on steel ball developed after sliding against glaze A coated Si_3N_4 flat

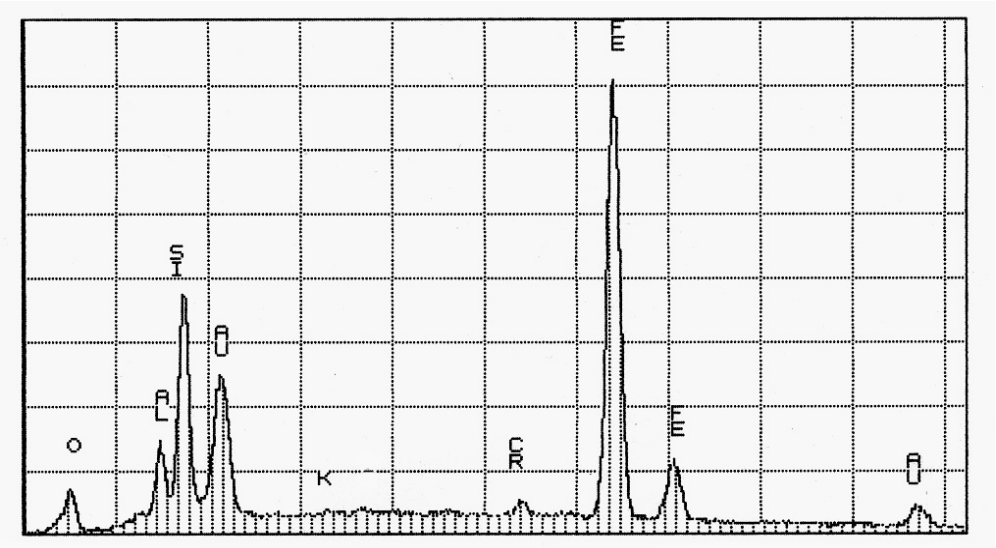

Figure 4.30 EDX spectrum of steel ball after sliding against glaze A coated Si_3N_4

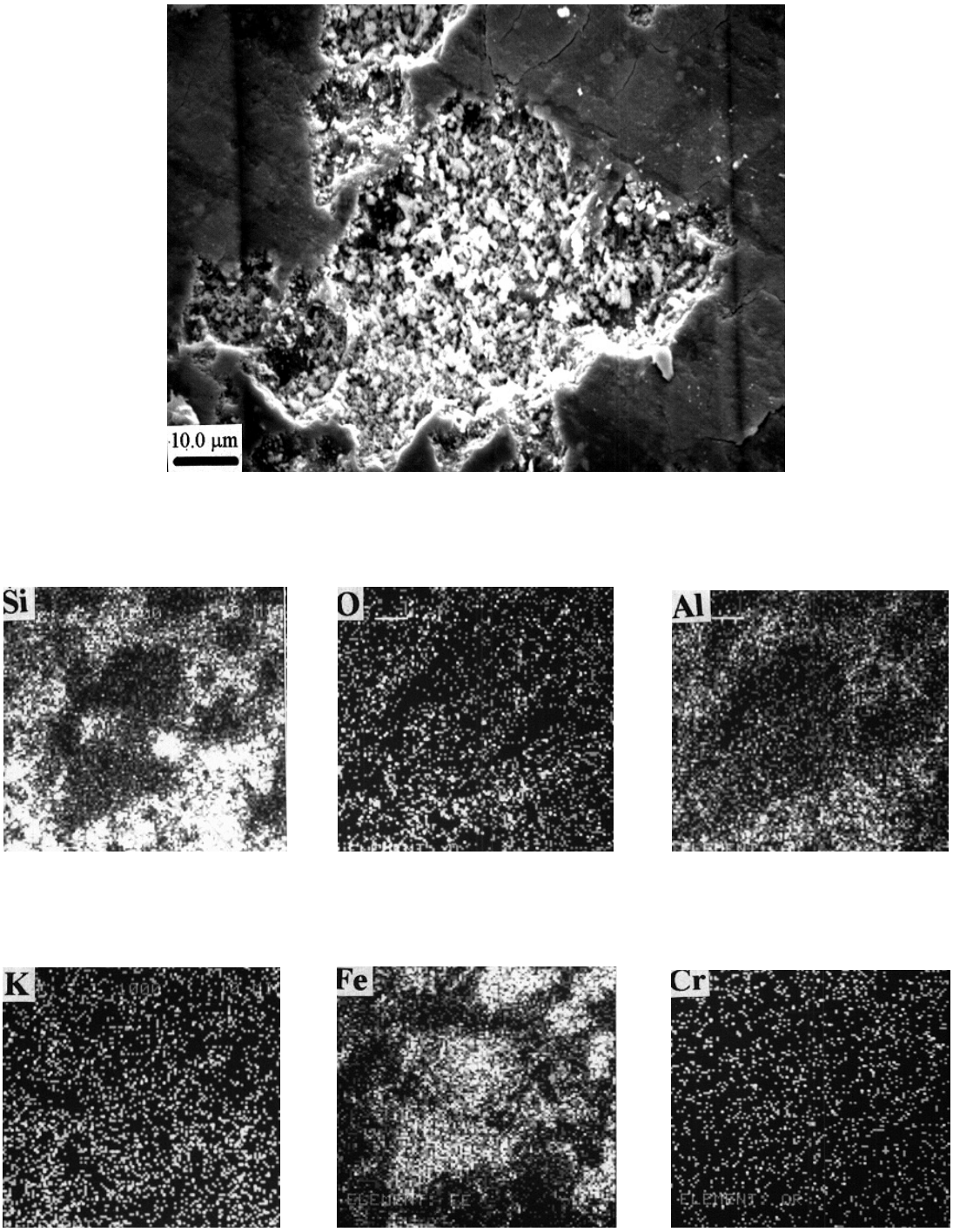

Figure 4.31 SEM micrograph and EDX elemental mappings of wear track on glaze A coated Si_3N_4 flat

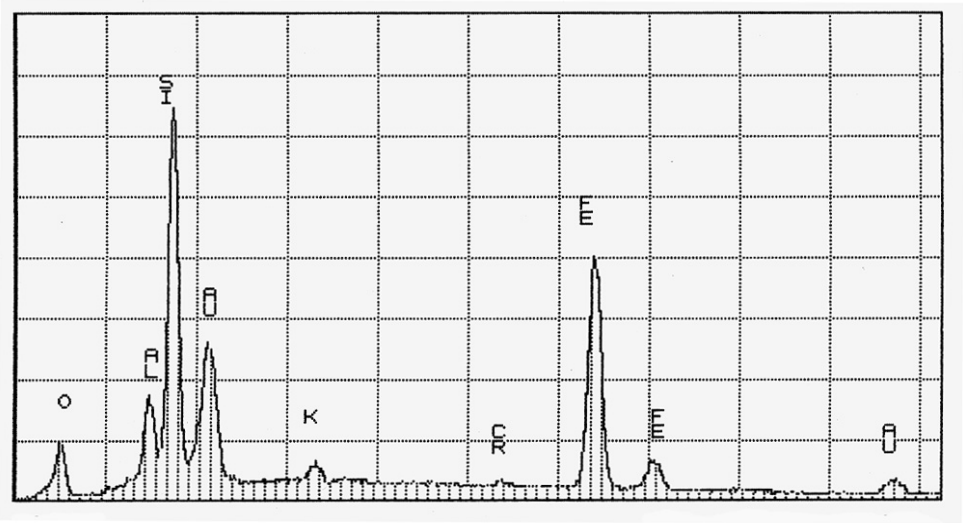

Figure 4.32 EDX spectrum of the wear track on glaze A coated Si_3N_4 flat

An overall view of the wear scar formed on the 52100 steel ball developed after sliding against the glaze A+Na_2SiO_3 coated Si_3N_4 flat specimen is shown in Figure 4.33. In this case, because of the unique donut shaped wear scar on the steel ball, EDX elemental mappings were done on the wear scar region which showed higher concentration of Si with a corresponding lower concentration of Fe along the outer and inner rims of the wear scar. The elements Na and O were uniformly distributed throughout the entire wear scar region. This implied that materials from the glaze had transferred to the steel ball. On the other hand, the wear of the glaze A+Na_2SiO_3 coated flat specimen was severe leading to a significant amount of coating material being removed due to the sliding of the steel ball against the flat specimen, shown in Figure 4.34. Iron transfer from the steel ball on to the Si_3N_4 specimen was very minimal as evident from the EDX spectrum shown in Figure 4.35. Based on the wear profile diagram (Figure 4.23) and the EDX spectrum (Figure 4.35), it can be inferred that the wear of the steel ball sliding against glaze A+ Na_2SiO_3 coated Si_3N_4 flat specimen was very insignificant. All these were expected to be observed because of the results obtained previously by running the surface profiler over the wear surface of the coated specimen.

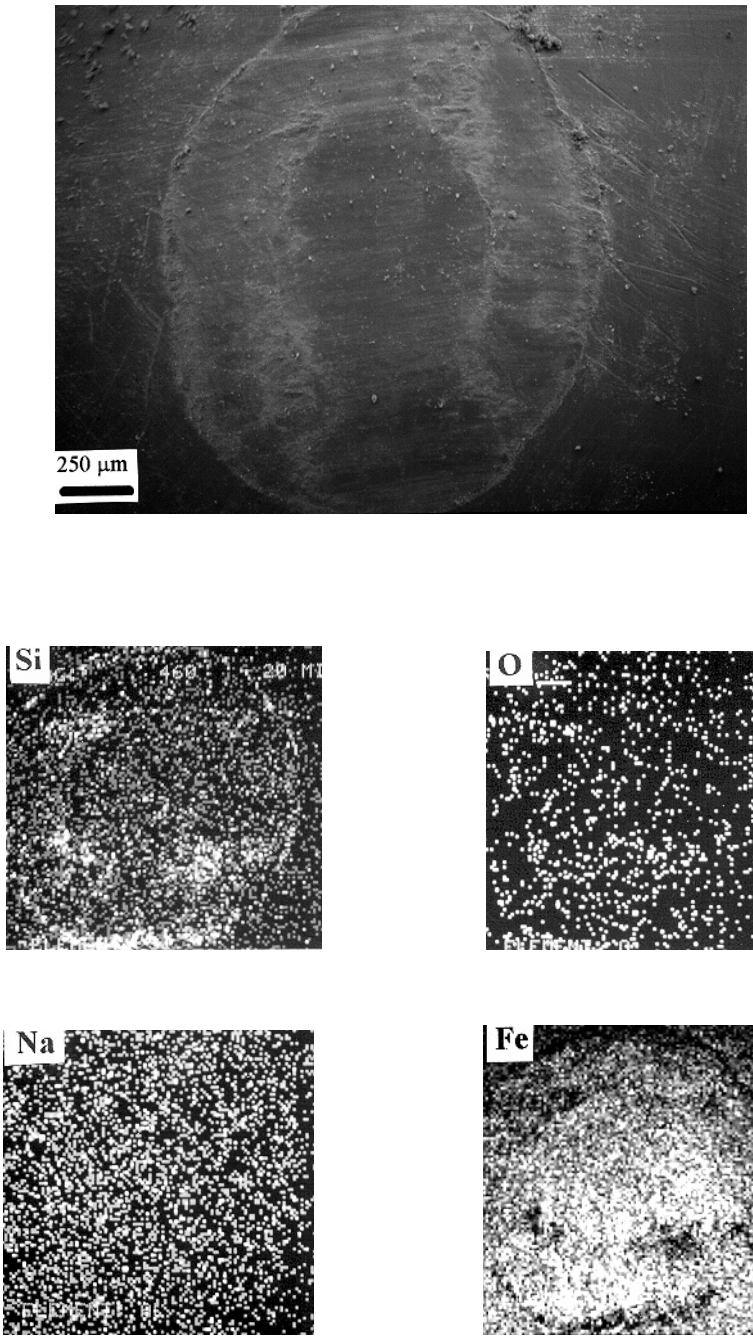

Figure 4.33 SEM micrograph and elemental mappings of wear scar on steel ball developed after sliding against glaze A+Na_2SiO_3 coated Si_3N_4 flat

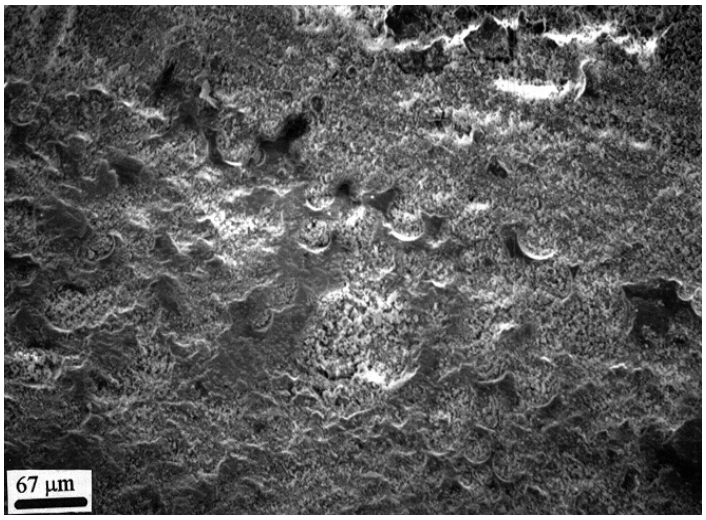

Figure 4.34 SEM micrograph of wear track on glaze A+Na_2SiO_3 coated Si_3N_4 flat

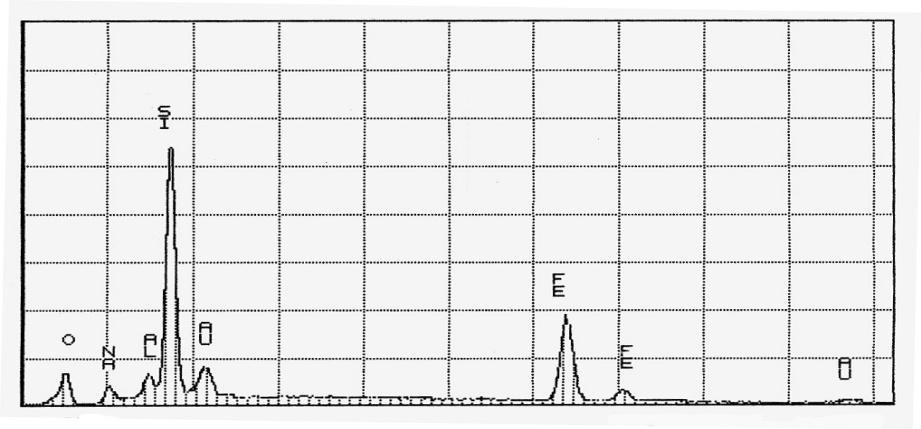

Figure 4.35 EDX spectrum of the wear track on glaze A+Na_2SiO_3 coated Si_3N_4 flat

The SEM micrograph of the wear scar formed on the steel ball sliding against glaze B coated Si_3N_4 flat specimen is shown in Figure 4.36. Similar to the previous two cases for glaze A and glaze A+Na_2SiO_3 coatings, the wear of the steel ball sliding against the glaze B coated Si_3N_4

Figure 4.36 SEM micrograph of wear scar on steel ball developed after sliding against glaze B coated Si_3N_4 flat

flat was lower than that observed for the uncoated one. However, if the EDX spectrum of the wear surface of the steel ball shown in Figure 4.37 is compared with that for the glaze A coated specimen (Figure 4.30), it can be said that a comparatively lesser amount of material was transferred from the glaze B coated Si_3N_4 flat specimen to the steel ball (by comparing the heights of Si peaks in the two cases). This indicated better adherence of the glaze B coating to the substrate as compared to glaze A. Figure 4.38 shows the SEM micrograph of a region along the wear track on the glaze B coated Si_3N_4 flat. As indicated by the associated X-ray maps, the wear debris along the wear track consisted mainly of material transferred from the steel ball.

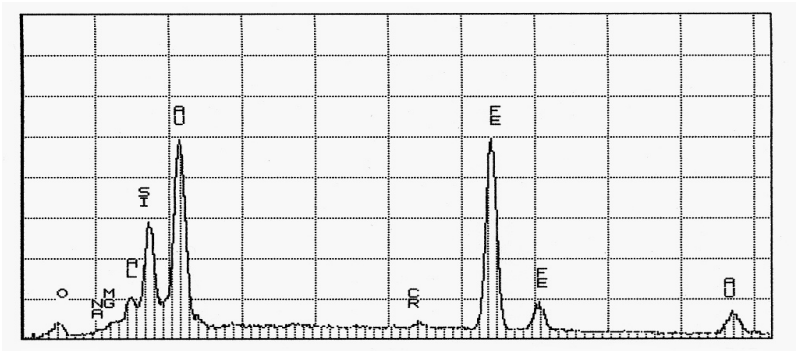

Figure 4.37 EDX spectrum of steel ball after sliding against glaze B coated Si_3N_4 flat

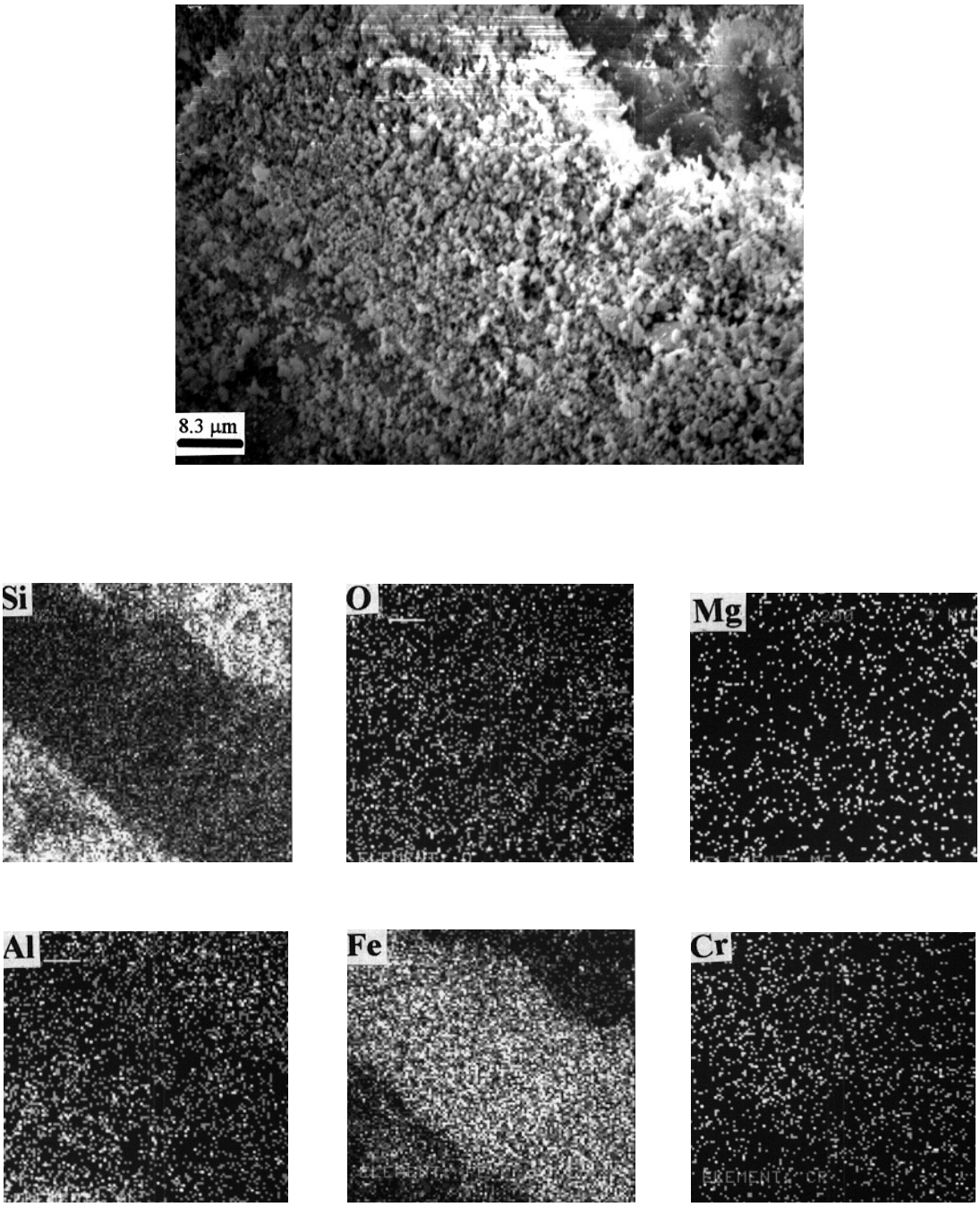

Figure 4.38 SEM micrograph and EDX elemental mappings of wear track on glaze B coated Si_3N_4 flat

The EDX spectrum of the glaze B coated Si_3N_4 flat wear surface given in Figure 4.39 shows greater amount of material transfer from the steel ball on to the Si_3N_4 flat than that for the glaze A coated specimen. This was evidenced by comparing the relative heights of the Fe peaks indicated in the EDX spectra corresponding to the wear surfaces of the glaze A and glaze B coated specimens.

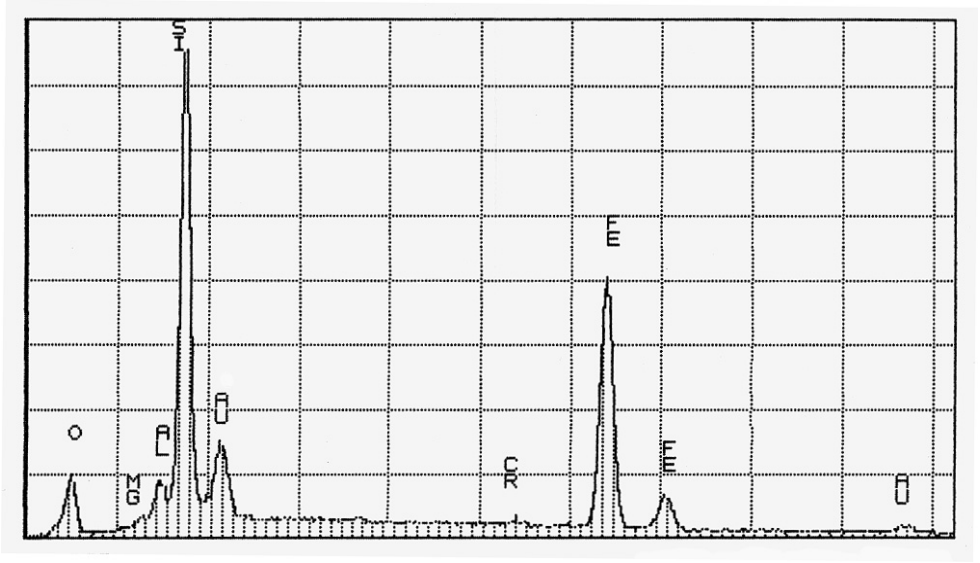

Figure 4.39 EDX spectrum of the wear track on glaze B coated Si_3N_4 flat

Table 4.5 compares the areas of the steel balls exposed during the wear tests performed on uncoated and coated Si_3N_4 flat specimens. It also shows the relative amount of Fe transferred from the steel balls on to the flat specimens. The exposed area of the steel ball would increase with an increase in the wear surface area. It was observed that, for the uncoated Si_3N_4 specimen, a large portion of the steel ball was exposed and a significant amount of Fe was transferred from the ball to the specimen. Hence, it can be qualitatively inferred that the uncoated Si_3N_4 specimen had a high wear resistance when tested against steel. Similarly, by observing the amount of Fe transferred from the steel ball on to glaze A and glaze B coated Si_3N_4 flat specimens, it can be

inferred that glaze B had higher wear resistance. The reductions in the exposed areas of the steel balls for glaze A and glaze B, when compared with uncoated Si_3N_4 specimen, indicate that the coatings are softer than Si_3N_4. In case of glaze A+Na_2SiO_3 coating, it was noted that, although a very large area of the steel ball was exposed, a very insignificant amount of Fe was transferred from the steel ball to the Si_3N_4 specimen. This implied that the coating was very soft (compared to glaze A and glaze B), and had a very low wear resistance.

Si_3N_4 flat specimens	**Exposed ball diameter (μm)**	**Fe transfer from ball to flat specimens**	**Wear resistance**
Uncoated	1050	High	High
Glaze A	625	Low medium	Low medium
Glaze A+Na_2SiO_3	1750	Low	Low
GlazeB	575	High medium	High medium

Table 4.5 Wear characteristics of uncoated and coated Si_3N_4 flat specimens

4.7 Summary of results

The glaze A coating formed homogeneous, crack-free, opaque and semi-crystalline glazed surface, 5 to 12μm thick with 1-3μm spheroidal grains. XRD analysis of the coated specimen revealed the presence of low expansion crystallized phases such as spodumene and eucryptite. Because the glaze A coated Si_3N_4 specimens did not develop a very smooth surface, a layer of sodium silicate was applied on the already matured LAS coated specimens and then subsequently fired. Although this led to the development of a smooth, glossy surface texture, fine cracks and bubbles were formed on the surface. The glaze B coating formed homogeneous, crack-free transparent glazed surface exhibiting a smooth and glossy appearance. The coating had a uniform thickness of about 9μm, with needle-like particles (8 to 12μm in size) of yttrium silicate. XRD analysis identified the crystallization of low expansion cordierite as the main phase.

The mechanical properties of the uncoated and coated as fired Si_3N_4 specimens were evaluated. It was found that all the coated specimens had greater room temperature flexural strength compared to the uncoated ones. Reasons for strength increment for each of the coating can be summarized as:

(i) glaze A+Na_2SiO_3 coating showed insignificant strength increment only because of the achievement of good surface smoothness. The formation of fine cracks and bubbles were the factors that hindered the strength of the coated materials to increase to any appreciable amount when compared to the uncoated ones.

(ii) glaze A coating was responsible for increasing the room temperature strength of the as fired Si_3N_4 by 21.2% because of the development of compressive stress at the surface of the specimen due to the low expansion spodumene and eucryptite phases in the glaze. This led to the reduction of the weakening effect of the surface flaws present on the uncoated as fired Si_3N_4 surface. In addition, the glaze coating was able to smooth out the surface defects by filling in the pores and holes present on the as processed surface of Si_3N_4.

(iii) glaze B coating resulted in maximum strength improvement of the as fired Si_3N_4 - by 44.5%. In addition to the formation of compressive surface stress due to the presence of low expansion cordierite phase, glaze B coating had achieved greater surface smoothness, had flowed well over the substrate surface penetrating into the surface voids/pits, had higher compressive stress, and thus had led to greater reduction of surface flaws and concomitant greater improvement in strength.

The coefficient of friction values (μ) obtained during the wear tests were found to be almost similar for all specimens. It was noted that the μ value was highest in case of the glaze A+ Na_2SiO_3 coating due to the maximum breakup of the glaze coating during the wear test. It was also observed that the wear resistance of the uncoated Si_3N_4 specimen was the highest. However, amongst the three coatings, glaze B coating exhibited maximum wear resistance followed by glaze A and glaze A+ Na_2SiO_3 coatings.

5.0 Conclusions

Glazing can be adopted as an inexpensive means to enhance room temperature flexural strength of as processed Si_3N_4. Fritted glaze coatings based on two different compositions LAS and MAS belonging to the ternary systems - lithia-alumina-silica (Li_2O-Al_2O_3-SiO_2) and magnesia-alumina-silica (MgO-Al_2O_3-SiO_2), respectively, were successfully formed on as fired Si_3N_4 substrates.

The LAS coatings formed homogeneous, crack-free, opaque and semi-crystalline glazed surfaces which improved the room temperature flexural strength by 21.2% over as processed Si_3N_4.

In an attempt to improve coating smoothness of LAS glazes, a layer of sodium silicate (Na_2SiO_3) was applied on the matured glaze A coated surface and then refired. However, this technique proved unsuccessful in significantly improving strength and wear resistance over as processed Si_3N_4.

MAS composition glaze on Si_3N_4 formed homogeneous, crack-free transparent coatings exhibiting a smooth and glossy appearance. The room temperature flexural strength of the MAS coated specimen was 44.5% greater than the as processed Si_3N_4.

Wear tests revealed that the wear resistance of the coated Si_3N_4 specimens were inferior to that of the uncoated. The wear resistance of the coated specimens were found to be decreasing in the following order: (i) MAS coating, (ii) LAS coating, (iii) LAS+Na_2SiO_3 coating.

6.0 Future Work

Although the current work involving the development of low expansion glaze coatings did result in enhancement of the room temperature flexural strength of as fired Si_3N_4, this research has been a preliminary study and there are issues that should be addressed in more detail.

The observation that the coatings did help to improve the flexural strength of the as processed Si_3N_4, was based on five tests for each of the three sets of coated specimens. It is desirable to conduct flexural strength measurements on a larger sample population in order to make more accurate statistical conclusions (like determining mean flexural strength values) and also to generate a reliable Weibull statistics.

In this research, single wear tests were performed for each of the uncoated and coated Si_3N_4 specimens. Future research should include more wear tests on each specimen in order to investigate thoroughly the effects of the coatings on the wear properties of the coated Si_3N_4 material.

In the present work it was found that, out of the two glaze compositions investigated, the magnesium aluminosilicate (MAS) glaze exhibited better coating characteristics than the lithium aluminosilicate (LAS) glaze. However, the MAS glaze had to be synthesized and processed at temperatures well above 1000°C. Future work should focus on the optimization of this MAS glaze composition to assist in lowering its synthesis and processing temperatures, and hence, develop a more cost effective glaze coating material.

One aspect in this research, that has been mentioned without being supported by quantitative analysis, deals with the compressive stresses produced on the surfaces of the coated

Si_3N_4 specimens due to glazing. It would be interesting to investigate the relative magnitudes of the compressive surface stresses by performing tests such as ring and rod tests.

The coefficients of thermal expansion (CTE) of the LAS and MAS glazes were calculated empirically. It would be useful to corroborate the calculated values by measuring the CTE of the glazes experimentally through the utilization of the dilatometric technique. Energy dispersive X-ray analyses (EDX) were used to determine the composition profiles of the surface layers. It would be more beneficial, though, if SIMS (Secondary Ion Mass Spectrometry) analyses are done in future, because SIMS provides better resolution and can detect a wider range of elements including lower atomic number elements such as Li.

References

1. K. Komeya, “Progress in silicon nitride ceramics in Japan,” Mat. Res. Soc. Symp Proc., 287 29-38 (1992)
2. Y. Hamano, “Progress in structural applications of silicon nitride,” Ceram. Trans. 42 3-14 (1994)
3. H. Takao, A. Okada, M. Ando, Y.Akimune, and N. Hirosaki, “Ceramics for reciprocating engines: an application review,” 4th Inter. Symp on Ceramic Matl. & Comp. for engines, 118-133 (1992)
4. R.R. Willis and R.E. Southam, “Ceramic engine valves,” J. Am. Ceram. Soc, 72[7] 1261-64 (1989)
5. S.Das and T.R. Curlee, “The cost of silicon nitride powder and the economic viability of advanced ceramics,” Am. Ceram. Soc. Bull., 71[7] 1103-11 (1992)
6. E.J. Kubel Jr., “Structural Ceramics : Materials of the future”, Advanced Matls. & Processes Inc. Metal Progress, 8 25-33 (1988)
7. H.P. Kirchner, Strengthening of Ceramics, Marcel Dekker, New York, NY (1979)
8. D.W. Richerson, Modern Ceramic Engineering, Marcel Dekker, New York, NY (1982)
9. M.M. Schwartz, Handbook of structural ceramics, McGraw-Hill, New York, NY (1992)
10. P.S. Myers, “Ceramics for transportation engines - siren or solution”, Appl. Mech. Rev., 42[3] 53-68 (1989)
11. Y. Tajima, “Development of high performance silicon nitride ceramics and their applications”, Mat. Res. Soc. Symp. Proc., 287 189-195 (1992)
12. B.D. Fabes and D.R. Uhlmann, “Strengthening of glass by sol-gel coatings”, J. Am. Ceram. Soc., 73[4] 978-88 (1990)
13. J.P. Singh, “A review of the effect of flaws on the fracture behavior of structural ceramics”, ANL / FE - 86 - 3 (1986)
14. H. Rawson, “Properties and Applications of Glass”, Glass Sci. & Tech., 3 98-138 (1980)

15. G.D. Quinn, J.J. Swab and M.J. Slavin, “Fractography of Glasses and Ceramics II”, Ceram. Trans., 17 309-361
16. H.P. Kirchner, R.M. Gruver and R.E. Walker, “Chemical Strengthening of Ceramic Materials”, Linden Laboratories,Inc. Summary Report, (1970)
17. S.I. Warshaw, “Pre-stressed Ceramics”, Am. Ceram. Soc. Bull., 36[1] 28,30 (1957)
18. B.R. Karstetter and R.O. Voss, “Chemical strengthening of glass-ceramics in the system Li_2O-Al_2O_3-SiO_2”, J. Am. Ceram. Soc., 50[3] 133-137
19. H.P. Kirchner and R.M. Gruver, “Chemical Strengthening of Polycrystalline Ceramics”, J. Am. Ceram. Soc., 49[6] 330-333 (1966)
20. H.P. Kirchner, R.M. Gruver and R.E. Walker, “Strengthening sapphire by compressive surface layers”, J. Appl. Physics, 40[9] 3445-52 (1969)
21. R.E. Bickelhaupt, “Diffusional Prestressing of ceramics”, Southern Institute Summary Report, Contract N00019-67-c-01518 (1968)
22. C.W. Parmelee, Ceramic Glazes, Cahners Publishing Company, Boston, MA (1973)
23. R.A. Eppler, “Glazes and Enamels”, Glass Sci. & Tech., 1 301-338 (1983)
24. G.C. Nelson, Ceramics, Holt, Rinchart and Winston, New York, NY (1960)
25. J.R. Taylor and A.C. Bull, Ceramics glaze technology, Pergamon Press, Oxford, UK (1986)
26. P.D. Prall, “Cordierite crystal-containing glaze”, U. S. Patent 4,287,260 (1981)
27. M.F. Barker, “Higher strength glass containers by flame spraying”, Glass Tech., 31[1] 25-27 (1990)
28. H.P. Kirchner, R.M. Gruver and R.E. Walker, “Strengthening alumina by glazing and quenching”, Bull. Am. Ceram. Soc., 47[9] 798-802 (1968)
29. E.F. O’Conor and R.A. Eppler, “Semicrystalline glazes for low expansion whiteware bodies”, Bull. Am. Ceram. Soc., 52 [2] 180-184 (1973)
30. R.A. Eppler and E.F. O’Conor, “Glazed ceramic ware”, U.S. Patent 3,804,666 (1974)
31. N.J. Kreidl, “Inorganic glass-forming systems”, Glass Sci. & Tech., 1 105-299 (1983)
32. M.B. Volf, Chemical approach to glass, Elsevier Science Publishers, New York, NY (1984)

33. K.W. Terry, “The use of spodumene in ceramic bodies and glazes”, J.Aus. Ceram. Soc., 25[1] 19-40 (1989)
34. J.H. Fishwick, Applications of lithium in ceramics, Cahners Publishing Company, Boston, MA (1974)
35. C.E. Brackbill, H.A. McKinstry and F.A. Hummel, “Thermal expansion of some glasses in the system Li_2O-Al_2O_3-SiO_2”, J. Am. Ceram. Soc., 34 107 (1951)
36. F.A. Hummel, “Thermal expansion properties of some synthetic lithia minerals”, J.Am. Ceram. Soc., 34[8] 235-239 (1951)
37. J. Hlavac, “Glass-ceramics”, Glass Sci. & Tech., 4 228-242 (1983)
38. M.D. Karkhanavaia and F.A. Hummel, “The polymorphism of cordierite”, J.Am. Ceram. Soc., 36[12] 389-92 (1953)
39. I.J. McColm, Ceramic science for materials technologists, Leonard Hill Publisher, New York, NY (1983)
40. S. Jahanmir, Friction and wear of ceramics, Marcel Dekker, New York, NY (1994)
41. S. Yang, “Corrosion resistant CMZP and Mg-doped Al_2TiO_5 coatings for SiC ceramics”, Master’s thesis, Dept. of Materials Science and Engineering, Virginia Tech, May 1996.
42. E.M. Levin, C.R. Robbins, and H.F. McMurdie (Eds.), Phase diagram for ceramists, American Ceramic Society, Columbus, Ohio, 1964
43. G.N. Babini, A. Bellosi, P. Vincenzini, “Factors influencing structural evolution in the oxide of hot pressed Si_3N_4-Y_2O_3-SiO_2 materials”, J. Mater. Sci., 19 3487-97 (1984)
44. L. Wang, C. He and J. Wu, “Oxidation of sintered silicon nitride”, Elsevier Sequoia, 125-130 (1992)
45. J. Eales, Manual and databook of glass technology calculations, Ordentlich, Holon, Israel (1977)
46. A.K. Varshneya, Fundamentals of inorganic glasses, Academic Press, London, UK (1994)
47. R. Tandon, Personal communication, Caterpillar, Inc.

Vita

Nandita Majumdar was born in Calcutta, India. In 1993, she received her M.Sc. degree in Geology from the University of Calcutta, Calcutta, India. She began her graduate studies in the Department of Materials Science and Engineering, Virginia Tech, in Fall 1996. She completed the requirements for M.S. degree in June, 1998.